

THERMAL PLASMA SYNTHESIS OF LSC-113/LSC-214 COMPOSITE  
CATHODE FOR IT-SOFCS

A THESIS SUBMITTED TO  
THE GRADUATE SCHOOL OF NATURAL AND APPLIED SCIENCES  
OF  
MIDDLE EAST TECHNICAL UNIVERSITY

BY

HAVVA EDA AYSAL

IN PARTIAL FULFILLMENT OF THE REQUIREMENTS  
FOR  
THE DEGREE OF MASTER OF SCIENCE  
IN  
METALLURGICAL AND MATERIALS ENGINEERING

SEPTEMBER 2019



Approval of the thesis:

**THERMAL PLASMA SYNTHESIS OF LSC-113/LSC-214 COMPOSITE  
CATHODE FOR IT-SOFCS**

submitted by **HAVVA EDA AYSAL** in partial fulfillment of the requirements for the degree of **Master of Science in Metallurgical and Materials Engineering Department, Middle East Technical University** by,

Prof. Dr. Halil Kalıpçılar  
Dean, Graduate School of **Natural and Applied Sciences**

\_\_\_\_\_

Prof. Dr. C. Hakan Gür  
Head of Department, **Met. and Mat. Eng.**

\_\_\_\_\_

Prof. Dr. Tayfur Öztürk  
Supervisor, **Met. and Mat. Eng., METU**

\_\_\_\_\_

...

\_\_\_\_\_

**Examining Committee Members:**

Prof. Dr. Kadri Aydınol  
Metallurgical and Materials Eng., METU

\_\_\_\_\_

Prof. Dr. Tayfur Öztürk  
Met. and Mat. Eng., METU

\_\_\_\_\_

Assoc. Prof. Dr. Hasan Akyıldız  
Metallurgical and Materials Eng., Konya Technical University

\_\_\_\_\_

Assist. Prof. Dr. Mert Efe  
Metallurgical and Materials Eng., METU

\_\_\_\_\_

Assist. Prof. Dr. Batur Ercan  
Metallurgical and Materials Eng., METU

\_\_\_\_\_

Date: 02.09.2019

**I hereby declare that all information in this document has been obtained and presented in accordance with academic rules and ethical conduct. I also declare that, as required by these rules and conduct, I have fully cited and referenced all material and results that are not original to this work.**

Name, Surname: Havva Eda Aysal

Signature:

## ABSTRACT

### THERMAL PLASMA SYNTHESIS OF LSC-113/LSC-214 COMPOSITE CATHODE FOR IT-SOFCs

Aysal, Havva Eda  
Master of Science, Metallurgical and Materials Engineering  
Supervisor: Prof. Dr. Tayfur Öztürk

September 2019, 55 pages

The current study follows the previous work in which a superior performance was obtained in the composite cathode  $(\text{La}_{0.8}\text{Sr}_{0.2})\text{CoO}_3$  (LSC-113) /  $(\text{La}_{0.5}\text{Sr}_{0.5})_2\text{CoO}_4$  (LSC-214) where the cathode was amorphous/nanocrystalline as a result of co-sputtering of the respective oxides. In the present work, cathodes of similar compositions were produced via thermal plasma and electrochemically characterized by impedance spectroscopy. The study has shown that nanopowders of LSC-113/LSC-214 can be synthesized via thermal plasma by feeding  $\text{La}(\text{NO}_3)_3 \cdot 6\text{H}_2\text{O}$ ,  $\text{Sr}(\text{NO}_3)_2$ ,  $\text{Co}(\text{NO}_3)_2 \cdot 6\text{H}_2\text{O}$  precursor solution. Nano powders obtained with RF thermal plasma with 25 kW were 58 nm in size and the Rietveld refined XRD pattern showed that the powder was a composite of LSC-113:LSC-214=0.3:0.7. The potential of the powder as cathode material was tested on a symmetric cell where the powder was applied either side of the electrolyte (GDC) and tested with impedance spectroscopy. Measurement conducted over a wide range of temperatures between 350-700°C. This has shown that the area specific resistance values of the cathodes made with synthesized powders were similar to those of co-sputtered cathodes. An ASR value of  $0.15 \Omega \cdot \text{cm}^2$  can be obtained in the current cathodes at temperatures as low as 665°C. A synthesis of LSC-113: LSC-214= 0.5:0.5 was recommended where

the operating temperature of the cathode could be reduced to temperatures less than 600°C.

Keywords: IT-SOFC cathode, LSC113/LSC214, RF thermal plasma, EIS, symmetric cell, composite cathode.

## ÖZ

### TERMAL PLAZMA İLE ORTA SICAKLIK KATI OKSİT YAKIT PİLLERİ İÇİN LSC-113/LSC-214 KOMPOZİT KATOD ÜRETİMİ

Aysal, Havva Eda  
Yüksek Lisans, Metalurji ve Malzeme Mühendisliği  
Tez Danışmanı: Prof. Dr. Tayfur Öztürk

Eylül 2019, 55 sayfa

Bu tezde, katı oksit yakıt pillerinin (KOYP) orta sıcaklıklardaki (500-700°C) performanslarının arttırılabilmesi için kompozit katot malzemeleri üzerine çalışmalar sürdürülmüştür. Katı oksit yakıt pillerinin performansları esas olarak kullanılan katotun kompozisyonundan ve mikro yapısından etkilenmektedir. Çalışma sıcaklığının düşürülebilmesi ve kinetiğinin hızlandırılabilmesi için, farklı kompozit katot üretim yöntemleri araştırılmıştır. Grubumuzda yapılan daha önceki bir çalışmada, eş zamanlı sıçratma çöktürme yöntemi ile üretilen  $(La_{0.8}Sr_{0.2})CoO_3$  (LSC-113) -  $(La_{0.5}Sr_{0.5})_2CoO_4$  (LSC-214) iki fazlı yapının amorf benzeri yapıya sahip olduğu ve KOYP'nin performansını arttırdığı gözlemlenmiştir. Bu çalışmada, LSC-113/LSC-214 kompozit katot, yüksek debide soğutma gazı kullanılarak termal plazma yöntemi ile yarı kararlı toz olarak sentezlenmiştir. Bu çalışmanın amacı, plazmada üretilen tozlar ile eş zamanlı çöktürme yöntemiyle üretilen katotların performanslarını karşılaştırılmasıdır. Bu amaçla, termal plazma ile sentezlenen iki fazlı oksitler (LSC-113:LSC-214) karakterize edilmiş ve molar fraksiyonları LSC-113:LSC-214=0.3:0.7 olarak bulunmuştur. Ardından, elektrokimyasal empedans spektroskopisi ölçümleri için simetrik hücre hazırlanmıştır. Bu ölçümler 350-700°C aralığında 50°C aralıklarla

yapılmıştır. Hedeflenen, alana özgül direnç değeri  $0.15 \Omega \cdot \text{cm}^2$  olarak alındığında, sentezlenen katodun  $665^\circ\text{C}$  sıcaklıkta kullanılabilmesi anlaşılmıştır.

Anahtar Kelimeler: Orta sıcaklıklı KOYP, LSC-113/LSC-214, simetrik hücre, RF termal plazma yöntemi, EIS

To my family...

## ACKNOWLEDGEMENTS

I would like to express my greatest appreciation to my supervisor Prof. Dr. Tayfur Öztürk for his guidance and support throughout this thesis work. His precious advices inspired me and enlightened my academic vision.

I am thankful to all the staff of the Metallurgical and Materials Engineering Dept. and I would like to thank to my lab mates; N. Özgür Darıcioğlu, Merve Ercan, Mehmet Mert Köse, Fahrettin Kılıç, Hilal Aybike Can, Aylin Elçi, Yiğit Akbaş, Necmi Avcı, Eren Şimşek and earlier members Fatih Pişkin, Cavit Eyövge, Sertaç Altınok and Pelin Livan.

I owe great debt to, Doğancan Sarı, Bengisu Sarı, Sıla Atabay Sıkan, Fatih Sıkan and Ayşe Merve Genç Ünalın for their endless support and being there whenever I need. I would also want to express my deepest gratitude to my dear friends Melike Tunçalp, Merve Özdil and Gökhan Can for their encouragement and motivation during my thesis studies. I will always remember their support.

Finally, and most importantly, I would like to thank my parents, Aynur Aysal and Mustafa Aysal for their endless support, patience, appreciation and encouragement throughout my entire life. I would like to express my deepest thanks to my brother Ersel Aysal who has always been my best friend and the biggest supporter in my whole life. I could not have complete this work without their support.

This study was financially supported by the Scientific and Technological Research Council of Turkey (TUBITAK) under Grant No. 114M128 and 217M628.

## TABLE OF CONTENTS

ABSTRACT .....	v
ÖZ .....	vii
ACKNOWLEDGEMENTS .....	x
TABLE OF CONTENTS .....	xi
LIST OF TABLES .....	xiii
LIST OF FIGURES .....	xiv
CHAPTERS	
1. INTRODUCTION .....	1
2. LITERATURE REVIEW .....	3
2.1. Solid Oxide Fuel Cells .....	3
2.2. Intermediate Temperature Solid Oxide Fuel Cells (IT-SOFCs).....	4
2.2.1. Anode and Electrolyte for IT-SOFCs .....	5
2.2.2. Cathode Materials for IT-SOFCs.....	12
2.2.2.1. Single Phase Cathodes .....	12
2.2.2.2. Composite Cathodes.....	18
2.3. Synthesis of Composite Cathode.....	19
3. EXPERIMENTAL PROCEDURE .....	23
3.1. LSC Composite Powder Synthesis via Radio Frequency Thermal Plasma ....	23
3.2. Material Characterization .....	26
3.3. Fabrication of Symmetric Cell .....	27
3.4. Electrochemical Characterization.....	28
4. RESULTS AND DISCUSSION .....	31

4.1. Characterization of LSC powder.....	32
4.2. Electrochemical Characterization .....	40
5. CONCLUSION .....	47
REFERENCES .....	49

## LIST OF TABLES

### TABLES

Table 2.1. Structural parameters for $\text{La}_{(1-x)}\text{Sr}_x\text{CoO}_{3-\delta}$ at $x=0.15$ and $0.3$ obtained with X-ray diffractometer by Sikolenko et al. [64], and $x=0.5$ with neutron diffraction by Das et al. [65] .....	16
Table 2.2. Structural parameter for of $(\text{La}(1-x)\text{Sr}_x)\text{2CoO}_{4-\delta}$ with $0.5 \leq x \leq 0.7$ by Andujar et al.[66] and $(\text{La}(1-x)\text{Sr}_x)\text{2CoO}_{4-\delta}$ with $0.375 \leq x \leq 0.75$ by James et al. [67] .....	17
Table 4.1. Concentrations of nitrates used for the preparation of precursor solution. ....	31
Table 4.2. Mole fractions of nitrates used for the preparation of precursor solution.	33
Table 4.3. EDS results of synthesized LSC powder. ....	33
Table 4.4. Lattice parameters of refined LSC powder after annealing. ....	38
Table 4.5. The cathode resistance and ASR values of LSC-113; LSC-214 in various temperatures. ....	42

## LIST OF FIGURES

### FIGURES

Figure 2.1. Schematic illustration of SOFC operation. ....	4
Figure 2.2. Conductivity of yttria-stabilized zirconia in air [37]. ....	9
Figure 2.3. Conductivity of yttria and scandia stabilized zirconia in air at 1000°C [37]. .....	10
Figure 3.1. Schematic illustration of the induction plasma system. ....	24
Figure 3.2. Schematic diagram of, a) the induction plasma torch, and b) the location of atomization probe. ....	25
Figure 3.3. Schematic drawing of symmetric cell in cross-sectional view. ....	27
Figure 3.4. Digital image of the screen-printing device. ....	28
Figure 3.5. Schematic representation of symmetric cell used in electrochemical impedance spectroscopy. ....	29
Figure 3.6. Assembly of the symmetric cell for EIS measurements in a split furnace. .....	29
Figure 4.1. Synthesized LSC powders by thermal plasma collected on filter. ....	32
Figure 4.2. SEM image of LSC powder a) synthesized, b) annealed powder. ....	32
Figure 4.3. TEM images of plasma synthesized LSC powder. ....	34
Figure 4.4. X-ray diffractogram of LSC powders a) new composite cathode, b) heated 1300°C for 1h. ....	37
Figure 4.5. Rietveld refinement of the X-ray diffractogram of powder synthesized by thermal plasma, with SrCO <sub>3</sub> phase. ....	38
Figure 4.6. Lattice volume of LSC-113 on Sr-doping dependence [64]. ....	39
Figure 4.7. Lattice volume of LSC-214 on Sr-doping dependence [66,67] ....	39
Figure 4.8. Cross sections of the symmetric cells produced with synthesized powder a) the complete cross-section b) The magnified image of LSC electrode applied to the surface. ....	40

Figure 4.9. Illustration of an EIS example observed in screen-printed symmetric cells for a)350, b)500, and c)700°C.....	41
Figure 4.10. The relationship between the log(ASR) vs 1000/T [K <sup>-1</sup> ] for LSC-113/LSC-214 composite cathode. The ASR values with P <sub>O2</sub> is also added for comparison. The solid points represent composite cathode under atmospheric condition and the hollow points represent the oxygen rich atmosphere. ....	43
Figure 4.11. The relationship between the log(ASR) vs cycle number at constant temperatures .....	44
Figure 4.12. X-ray diffractogram of powder synthesized by induction thermal plasma after 700°C 1hour annealing. XRD pattern of as-synthesized powder as well as that of powder annealed 800 °C for 5 hours are also included for comparison.....	45



## CHAPTER 1

### INTRODUCTION

Fuel cells are promising alternative energy conversion devices to be used in many application areas. Among them, solid oxide fuel cells (SOFCs) have a special place in energy production, since they have advantages of fuel flexibility and high operating efficiency. Also, they do not require precious metal catalysts and only produce heat and water as by-products. However, they have relatively high operating temperatures causing the high energy input and a long start-up time [1]. These high operating temperatures also cause problems such as corrosion, durability, degradation etc. Therefore, the efforts are focused on reducing the operating conditions of SOFC. This allows more rapid start-up and shut-down, reduced corrosion rate for metallic components, and improved durability.

However, there are two problems that must be solved in reducing the operating temperature of the SOFCs; reduction of the high ohmic resistance of electrolyte and development of high-performance cathodes compatible with the electrolyte material. There are several approaches to lower the operating temperatures. These are thinner electrolyte with a high ionic conductivity, and the other is to use mixed ionic and electronic conducting cathodes, i.e. MIEC.

The choice of electrolyte is quite critical and in that respect the choice of GDC ( $\text{Ce}_{0.9}\text{Gd}_{0.1}\text{O}_{2-x}$ ) with ionic conductivities in the order of  $10^{-2}$  S/cm satisfies requirements as an electrolyte for temperatures as low as 600°C [2].

The improvements in cathode performance can be achieved through the use of mixed conducting perovskite-type oxides. Since, LaSrCoO (LSC) based perovskites have always been the best regarding both ionic and electronic conductivities. And they are compatible with the GDC electrolytes. Moreover  $\text{La}_{1-x}\text{Sr}_x\text{CoO}_{3-\delta}$  (LSC-113) and  $(\text{La}_{1-x}$

$x\text{Sr}_x)_2\text{CoO}_{4-\delta}$  (LSC-214) dual phase cathode were demonstrated by Crumlin et al. [3] and Sase et al. [4] to exhibit improved electrochemical performance. This was attributed to the presence of hetero-interfaces, which enhances oxygen surface exchange. Thus dual phase LSC-113 / LSC-214 cathodes provide a relatively high effective oxygen fluxes as a result of high surface exchange and superior oxygen diffusivities. This results in improved oxygen reduction reaction (ORR) in the cathode [5]. Sari et al. [6], used the co-sputtering technique which is utilized due to the apparent advantage of hetero interfaces, in order to improve cathode materials with better performance at intermediate temperature range. According to the study, it can be said that the compositions that are in the certain volume fraction range have important role to improve cathode performance.

There are variety of methods to produce the perovskite-type oxides and each method could result in different structure, particle morphology, surface area, and the amount of hetero interface. The wet production methods are mostly used in synthesis of cathode material for SOFCs. In these processes, the nitrate based compounds are mixed in certain amounts to obtain the gel form. The gel is then dried at certain temperature and calcined at high temperatures. These methods mostly require high temperature and take a long time [7]. As an alternative method, the cathode materials can be synthesized via thermal plasma [6, 7]. This method provides an efficient way to synthesize the uniformly distributed composite nanopowders, without any mechanical mixing processes [10]. In this approach, powder was synthesized from a precursor solutions prepared by mixing nitrates, oxides and carbonates of desired proportions.

The current study follows the previous work on sputter deposited composite cathode and aims to compare their cathode performances with thermal plasma synthesized dual phase oxides. After fabrication, electrochemical impedance spectroscopy (EIS) is conducted to compare their performances.

## CHAPTER 2

### LITERATURE REVIEW

#### 2.1. Solid Oxide Fuel Cells

A schematic representation of SOFC is given in Figure 2.1. As seen in the figure the cell consists of three components; cathode, electrolyte and anode. In cathode side, oxygen is reduced  $1/2O_2 + 2e^- \rightarrow O^{2-}$  and goes through a dense electrolyte to anode, where it combines with the fuel  $2H^+ + O^{2-} \rightarrow H_2O$  to generate water. Since electrolyte is electronically not conductive, electron goes through the external circuit generating power.

Since, reduction reaction occurs in the cathode side, the cathode must be stable in oxidizing environment. It also should have sufficient catalytic activity and electronic conductivity. They also must have thermal and chemical compatibility with the electrolyte, which are in direct contact with.

The electrolyte should not allow passage of the gas on either side. It must be very thin and chemically stable under oxidizing and reducing atmospheres [10,11]. The most importantly it must have good ionic conductivity, because the oxygen ion passes through it and its electronic conductivity should as low as possible.

Since anode is directly in contact with the fuel, it may be called as a fuel electrode. In the anode side, fuel is distributed over entire surface, so it must have a porous structure. A suitable anode should carry the protons to the electrolyte where they come across with oxygen ions. The anode should have high electronic conductivity.

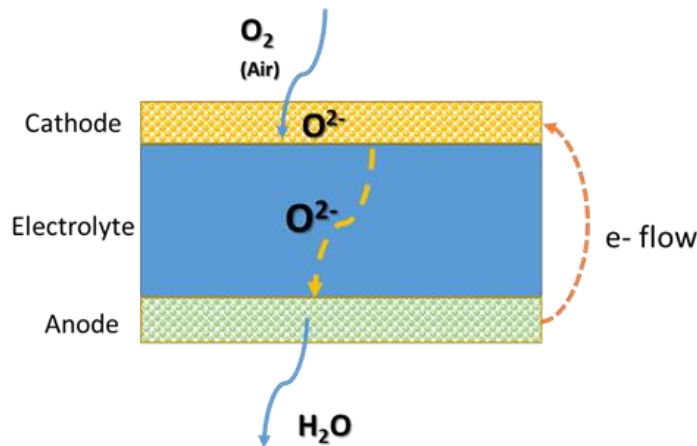


Figure 2.1. Schematic illustration of SOFC operation.

Components, as described above, must be chemically and mechanically stable during operation. Each component must perform in harmony to decrease the thermal stresses while start-up and shut-down. Thus the components should have minor mismatch in their thermal expansion coefficients (TEC). The material selection is therefore, the cornerstone of development of an high efficiency and durable SOFCs.

## 2.2. Intermediate Temperature Solid Oxide Fuel Cells (IT-SOFCs)

SOFCs are operated at high temperatures to ensure rapid kinetics and fast ion transport. Also, electrodes have high conductivity at high temperature range (800-1000°C), the kinetics associated with cathode reactions are sufficiently rapid and the cell losses are minor [13].

However, this high temperature has some drawbacks. Degradation of material performance at high temperature is one of the major problem. In addition, during start-up and shut-down, damage may be caused by thermal stresses which requires care in the operation. The material costs are also high. Therefore, there has been a great interest in lowering the operating temperature of the SOFCs to intermediate temperatures, i.e. the so called IT-SOFCs [12,13].

The main advantage of decreasing the operating temperature is rapid start-up and shut-down resulting improved durability with reduced corrosion rate [9]. However, lower

operating temperature decreases the electrode kinetics. The main problem is ORR at cathode which becomes quite slow [15].

Hence, alternative materials development at lower temperature is an important step in development of IT-SOFCs.

### **2.2.1. Anode and Electrolyte for IT-SOFCs**

Anode is located where, reduced oxygen meet with fuel provided and exhausting gases forms. For better anode performance, easy flow of electrons is helpful. So, the main requirement for anode part of SOFC is high electrical conductivity. For this reason, cermets are commonly chosen as anode materials; i.e. mixing oxides with a metallic compound. Additionally, high and stable porosity is necessary for more efficient penetration of fuel into anode as well as for the exhaust of the gas output.

For fuel oxidation process there is an activation energy, which is relatively small in overall resistance of SOFC. To reduce this resistance, anode should be able to catalyze fuel oxidation process, which can be handled partly by introduction of three-phase boundary (TPB) [16]. Anode is expected to be sufficiently strong to endure the weight of cell, since cell is anode supported in most cases. The oxide used in anode cermets is generally the same oxide which is used as electrolyte while metallic component can be either nickel, cobalt or iron.

One of the most common anode material is yttria stabilized zirconia (YSZ) based cermets. Since they are compatible with YSZ electrolytes, they increase the chemical and mechanical compatibility. Necessary electronic conductivity is mostly procured by metallic components like cobalt, nickel or iron. However, cobalt based cermets have high cost and the iron based cermets have corrosion problem under reducing atmosphere [16, 17]. Thus, nickel is the mostly selected metal to obtain YSZ based cermet anodes.

Zhu et al. [19], studied that the electronic conductivity enhancement of the anode by increasing Ni amount up to ~40 vol %. After this point there was a decrease in

conductivity. In Ni-YSZ anodes, Chen et al., [20] has shown that there is a drastic reduction of TPB with coarsening of Ni. In order to enhance the life time of the anode, the YSZ amount in the cermet should be relatively high. They indicated that the 45 vol % Ni loading is the best. On the other hand, when Ni loading increased up to 55-60 vol % the electrode activities also increased, but the performance of cell operation decreased due to the sintering of Ni particles. While Ni is lower than 35 vol %, TPB decreases due to insufficient Ni. According to Lee et al. [21], for best performance is obtained when NiO and YSZ have similar particle sizes.

Ni-YSZ anodes are well assembled anode materials, when the fuel is hydrogen. However, for the use of hydrocarbons Ni-YSZ anode fails as nickel catalyzes the carbon formation [15]. In order to prevent carbon formation, nickel is replaced with copper. Considering stability and cost under reducing conditions, copper is one of the best alternative among other metals.

Cu and Ni bearing cermets are investigated in a number of studies as anode materials. The effect of Ni-Cu alloying was investigated with regard to the performance and stability of YSZ anode for direct oxidation of methane [22]. They found that the alloy composition, which has 80% Cu, was yielding the best performance as power density. They also resulted that the Cu-Ni alloys are greatly suppress the carbon formation compared to pure Ni. In a similar study the same alloys were also found to be useful for reducing carbon deposition on ceria based anodes [23].

Ceria is examined as an alternative anode instead of zirconia, which is suitable for hydrocarbon based fuels. The ceria have the same structure with YSZ in terms of oxygen deficiency, similarly doped with rare earth elements. It is also resistant to sulfur poisoning which might be present in the fuel [24].

Comparison of the degradation rate of Ni-YSZ and Ni-GDC cermets on oxidation-reduction conditions, proven that the mechanism was different in two systems. Below 850°C, Ni-YSZ system exhibits a stable performance, but they still continue to degrade. At relatively low temperatures, as an alternative, Ni-GDC can be selected.

Lee et al. [25], have investigated these two systems to compare for direct oxidation of methane under conditions of catalytic partial oxidation. According to their results, Ni-GDC shows higher power densities ( $1.35 \text{ W/cm}^2$ ) than Ni-YSZ ( $0.27 \text{ W/cm}^2$ ) anodes at  $650^\circ\text{C}$ . In addition, they also reported that a slight degradation was observed in terms of performance on Ni-YSZ system, while Ni-GDC system was stable over long time operation. They noted the GDC use suppresses the carbon poisoning of Ni, thus operation becomes more stable.

In a similar work Zhang et al. [26], compared sulfur poisoning in GDC and YSZ at  $800^\circ\text{C}$ . The performance and activity of these anodes are examined with various  $\text{H}_2\text{S}$  contents. As a result, the anode potential in both cermets have decreased when  $\text{H}_2\text{S}$  contents increased. They noted that the Ni-YSZ anode has less tolerance to sulfur poisoning than Ni-GDC anode.

Anode stability is of importance in SOFC operation, so the stability was studied in the existence of water vapor. Gorte et al. [27], found that Cu-GDC had a maximum power density of  $0.15 \text{ W/cm}^2$  compared with  $0.03 \text{ W/cm}^2$  for Cu-YSZ. Cu-samarium doped ceria (SDC) also compared with Cu-YSZ systems with two types of fuels, hydrogen and propane [26]. The maximum power density of Cu-SDC system was higher than that of Cu-YSZ with both fuels. In addition, Cu-SDC anode has the lower anodic polarization resistance according to electrochemical impedance spectroscopy measurements.

Double perovskites are also studied as possible anode materials for SOFCs in the temperature range of  $650\text{-}1000^\circ\text{C}$ . Among the anode materials in the literature,  $\text{Sr}_2\text{MgMoO}_{6-y}$  found to be stable for 2 days operation, resulting  $642 \text{ mW/cm}^2$  at  $750^\circ\text{C}$  with hydrogen as a fuel, without sulfur or carbon formation. In other double perovskite systems,  $\text{A}_2\text{FeMoO}_{6-\delta}$  where  $\text{A} = \text{Ca}, \text{Sr}, \text{Ba}$  have also been studied, and the performance of cells was found to decreases from Sr to Ca, with the same electrolyte and cathode [28].

Hence, Ni/YSZ composite is the most commonly used anode for SOFC as it satisfies almost all requirements for anode applications with the exception of fuel flexibility [28–30]. However, Cu-GDC seems to display better resistance to carbon formation and sulfur poisoning, especially in 500-600°C.

It should be noted that, the electrolyte has the central part in SOFC. The solid electrolytes should have a good number of properties to be used for fuel cell. Therefore, it should have high oxygen ionic conductivity, since they are responsible for the transport of reduced oxygen ions. It is also necessary that they should have the lowest possible electrical conductivity to reduce losses from current leakage. According to Biswas et al. [32], the lower limit is around 600°C, when the operating temperature reaches this limit the ionic transport resistances of the electrolyte starts to increase and affects the cell performance.

In most cases, an ionic conductivity level of 0.01 S/cm is accepted as sufficient at current operation temperature for SOFC electrolytes [32,33]. Electrolyte should also be dense and thin, since porosity is not desired for efficient ion transport. It also should be stable both at oxidizing and reducing conditions. When the materials are choosing, the attention must be paid to many parameters; i.e. gas tightness, electronically non-conducting, chemical stability over a wide oxygen partial pressure and temperature range. Generally used electrolyte materials are scandium stabilized zirconia (ScSZ), yttrium stabilized zirconia (YSZ), and gadolinium doped ceria (GDC).

Zirconia has the cubic structure at higher than 2300°C, thus divalent and trivalent cation dopant is needed to stabilize its crystal structure at lower temperatures. Ceria shows the fluorite structure by forming solid solutions with divalent and trivalent cations, at room temperature [32]. Although the most common dopant is the yttria, the alternative candidates are calcia and scandia, i.e. calcia - stabilized zirconia (CSZ) and scandia-stabilized zirconia (ScSZ).

Among all candidates, the oxygen deficient fluorite structure is obtained in  $\delta$ -Bi<sub>2</sub>O<sub>3</sub>. For that reason,  $\delta$ -Bi<sub>2</sub>O<sub>3</sub> has superior conductivity. Despite that,  $\delta$ -Bi<sub>2</sub>O<sub>3</sub> have

chemical instability at high temperature, which means it is easily reduced and decomposed to bismuth metal at low oxygen partial pressure [34,35]. Consequently, the use of  $\delta$ -Bi<sub>2</sub>O<sub>3</sub> is uncertain as an electrolyte material for SOFC. Thus, ceria and zirconia-based materials seems better for the application of SOFC electrolyte.

Over broad range of temperature, stabilized zirconia remained stable, and the ionic conductivity was not affected by oxygen partial pressure. As an electrolyte material YSZ is commonly used, since it has high ionic conductivity. The ionic conductivity has reached the highest value when 8 mole % of yttria is doped. Increasing with the dopant level, the stability of cubic structure is improved. In terms of electronic conduction, YSZ is a nearly perfect insulator. It seems to YSZ has the best electrolyte candidate at high operating temperature. However, the ionic conductivity of YSZ is less than adequate when the operating temperature is in the range 500-700°C, Figure 2.2 [37].

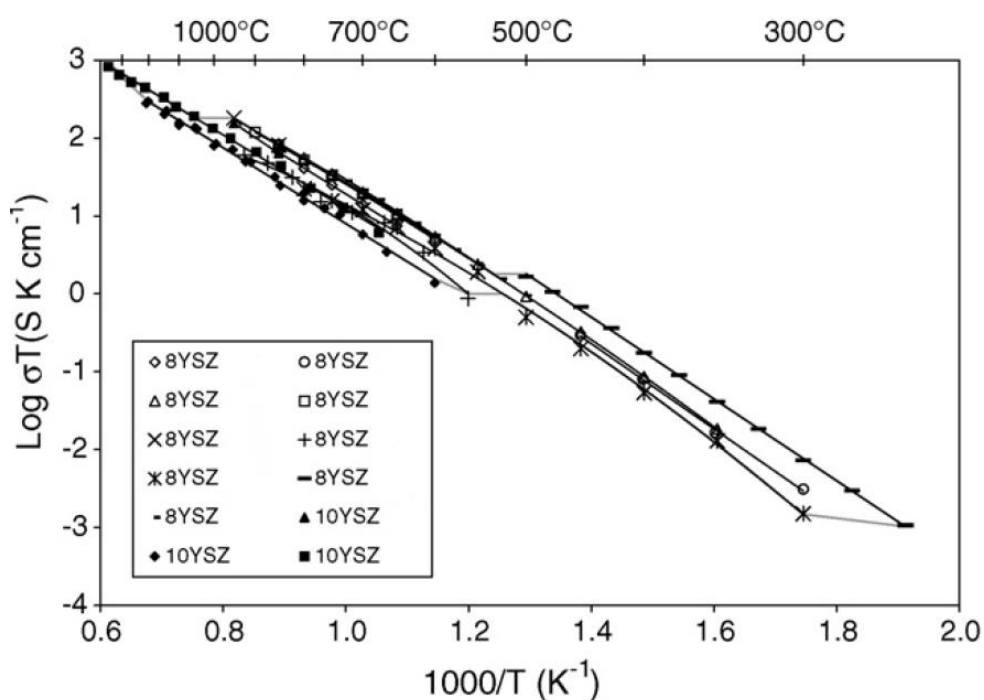


Figure 2.2. Conductivity of yttria-stabilized zirconia in air [37].

Another promising dopant for zirconia is scandia. It has higher conductivity than YSZ, Figure 2.3. The activation energy for ScSZ conduction tends to increase with decreasing temperature, such that the conductivity of ScSZ is similar or even lower than that of YSZ below 500°C. So, YSZ/ScSZ/YSZ layered electrolyte is designed for IT-SOFCs. ScSZ provides great ionic conductivity when thin YSZ brings electronic insulation and chemical stability. Therefore, it is seen that scandium stabilized zirconia is the best candidate at low temperature range. On the other hand, scandium increases the material cost.

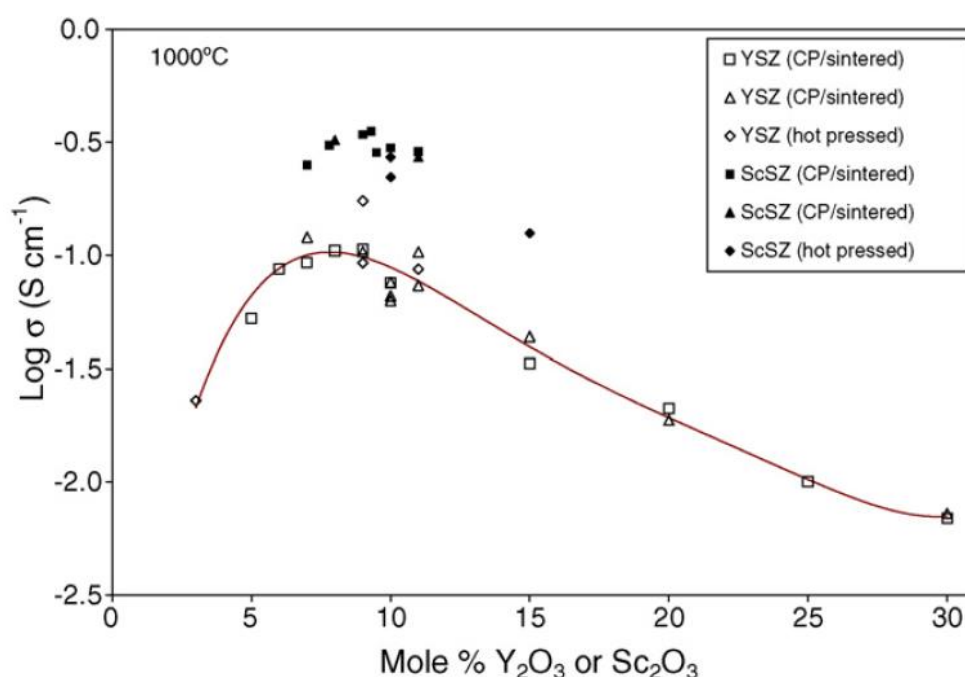


Figure 2.3. Conductivity of yttria and scandia stabilized zirconia in air at 1000°C [37].

According to Cho et al. [38], ScSZ single layer thin film of electrolyte gives an outstandingly high ionic conductivities than YSZ, but electronically YSZ has more resistive than ScSZ. Badwal et al. [39] found that the doping level of ScSZ higher than 9 mole % leads to a more stable system. Moreover, while heating and cooling when the doping level is higher than 9 mole %, a rhombohedral phase did form which negatively affected the ionic conductivity. Thus the optimum composition is obtained as 9.3 mole % scandia.

Zirconia based electrolytes have the main problem, which is reactivity with some of the barium or lanthanum bearing electrodes. To prevent this, the buffer layers are commonly used between the electrolyte and the electrodes.

Another common electrolyte material is the  $Ce_{1-x}Gd_xO_2$  (CGO) for IT-SOFCs. Like zirconia, ceria is doped to increase conductivity, and the highest conductivity occurs for ions with the lowest size mismatch, which is gadolinium and samarium for cerium. The conductivity of CGO is higher than those of YSZ and ScSZ below 600°C. Similar with zirconia, the conductivity increases with increasing dopant concentration to a maximum (e.g.  $x=0.20-0.25$  Gd) and then decreases. However, electronic conductivity of ceria is not as low as ScSZ or YSZ.

Another common group of electrolytes are the perovskite type electrolytes. Lanthanum gallate have quite high potential, but requires an isolating layer because of its reactivity with anode. As a buffer layer lanthanum nickelate ( $LaNiO_3$ ) is used [40]. In general, lanthanum or gadolinium doped ceria is used as a buffer layer to anode facing side of the electrolyte. A comparison between GDC and LDC ( $La_{0.4}Ce_{0.6}O_{1.8}$ ) carried out by Gong et al. [41], concluded that LDC has more efficient as a buffer layer.

Another method of enhancing the conductivity in ceria based electrolytes is forming composite electrolyte using inorganic salts; chlorides or carbonates. In this way, dissimilar interface areas between the salt phase and doped ceria phase are enhanced. This gave a power density of as high as 350 mW/cm<sup>2</sup> at 600°C [42]. As pointed out by Zhang et al. [26], the power density of the ceria-carbonate based system is not stable and decreases gradually with time, as a result of interaction between the phases. Therefore, in terms of chemical stability, the ceramic-carbonate based composite electrolytes need to be improved. Al or Mg doped titanates show high oxide ion conductivity; i.e.  $CaTiO_3$ . However, their ion conductivity is lower than that of YSZ. So, they are not suitable for IT-SOFC application [32].

In conclusion, even though new systems are being developed, GDC based oxides are still the most popular electrolytes for IT-SOFCs.

### 2.2.2. Cathode Materials for IT-SOFCs

The cathode is responsible for the reduction of the oxygen and transport the oxygen ions into the electrolyte. They should be electrically conductive and normally porous. In addition, they preferably should have high ionic conductivity to obtain the ionic diffusion through the cathode. As it is known, the oxygen molecules are provided to the cathode surface mostly from air, and reduced to oxygen ions ( $O^{2-}$ ). This reaction is often called as oxygen reduction reaction ;



Reduced oxygen ions are transported to the electrolyte which then crosses through to the anode side. This oxygen reduction reaction taking place at the cathode has significantly high activation energy making this the main rate limiting step in overall SOFC operation [9,40,41,44].

Since the oxygen reduction reaction (Eq 2.1) occurring at the cathode has a high activation energy, decreasing the operating temperature makes the cathode into the major source of electrical losses for the whole system as extensively reviewed, for instance, by Fleig et al.[45].

#### 2.2.2.1. Single Phase Cathodes

Single phase cathodes used for IT-SOFC are mainly based on perovskites; LSM ( $La_{1-x}Sr_xMnO_3$ ), LSCF ( $La_{1-x}Sr_xCo_{1-y}Fe_yO_{3-\delta}$ ), BSCF ( $Ba_{1-x}Sr_xCo_{1-y}Fe_yO_{3-\delta}$ ), LNF ( $LaFe_{1-x}Ni_xO_{3-\delta}$ ), LSC ( $La_{1-x}Sr_xCoO_{3-\delta}$ ).

In this type of oxides,  $ABO_3$ , the total charge of cations is +6. When the total valence is less than six, there is a missing charge which presents vacancy at the oxygen lattice sites [24,46,47]. Here the A-site cation is a combination of rare earths (La, Sr, Ca, or

Ba) and alkalines. The B-site is formed from reducible transition metals such as manganese (Mn), cobalt (Co), iron (Fe), and nickel (Ni).

LSM ( $\text{La}_{1-x}\text{Sr}_x\text{MnO}_{3-\delta}$ ) is traditionally used as cathode for SOFCs because of their high electronic conductivity, good chemical stability under oxidizing atmospheres. However, the cathode reaction is limited to a narrow three-phase boundary (TPB) region; where the air, cathode and electrolyte are in contact [48]. The electronic conductivity of LSM increases with the amount of Sr doping, until 50 mole % [36]. In general, the electrical property of LSM is not adequate when the operating temperature is lower than 800°C. The reduction of oxygen is limited to the TPB regions, because of the absence of oxygen vacancies in LSM. This limitation is the main reason for unsatisfied performance of LSM at lower temperatures. In order to use the LSM cathodes at lower temperatures, there are two approaches have been applied [36]. First one is to combine the LSM with additional phase which is ionically conductive. This additional phase widens the surface area of the cathode, resulting enhancement in ORR. Other approach is to change lanthanum with rare earth elements. Cation doping in LSM also encourages the oxygen vacancy formation, which supports the oxygen reduction kinetics [47].

LSCF shows good electrical conductivity and a high oxygen self-diffusion coefficient in between 600 and 800°C. The oxygen self-diffusion coefficient of LSCF is  $2.6 \times 10^{-9}$  cm<sup>2</sup>/s at 500°C, that is greater than  $\text{La}_{0.8}\text{Sr}_{0.2}\text{MnO}_3$  which has an oxygen self-diffusion coefficient of  $10^{-12}$  cm<sup>2</sup>/s at 1000°C [29]. Additionally, LSCF has no reactivity with ceria-based electrolytes [49]. Usually, the increase of ionic conductivity is influenced by Sr concentration at the A-site while the increase of the electronic conductivities is more influenced by Fe and Co concentration at the B-site. The A-site deficiency has only a small effect on the TEC while a higher Sr content results in a higher TEC due to higher oxygen vacancy concentrations. Mai et al. [50] observed that a small A-site deficiency and a high strontium content had a positive effect on the cell performance using LSCF as a cathode material. The measured current density of cells consisting of

LSCF cathode was  $1.76 \text{ A}\cdot\text{cm}^{-2}$  at  $800 \text{ }^\circ\text{C}$  and  $0.7 \text{ V}$ , which is twice of the cells with LSM/YSZ cathodes.

As pointed out by Uhlenbruck et al.[51], LSCF-based cathodes have superior properties to LSM-type cathodes, since LSCF-based cathodes have lower area specific resistance at lower operation temperatures. Since the LSCF has the undesirable interface reactions with YSZ, LSCF-type perovskites have compatibility problem with YSZ electrolytes. CGO barrier layer is used in order to inhibit the formation of low conductive compounds that can be negatively affect the electrochemical performance. Another reason for greater degradation rates for LSCF cathode cells lies in the diffusion of strontium from LSCF, leading to strontium discharge in the cathode, resulting in markedly reduced performance. Cells with slightly less Sr in the cathode ( $\text{La}_{0.58}\text{Sr}_{0.38}\text{Co}_{0.2}\text{Fe}_{0.8}\text{O}_{3-\delta}$ ) were found to perform less than  $\text{La}_{0.58}\text{Sr}_{0.4}\text{Co}_{0.2}\text{Fe}_{0.8}\text{O}_{3-\delta}$  [55,56]. Partial decomposition of perovskite has been found to generally have a greater effect on cell degradation rather than interface reactions during processing.

Wei et al. [54], used BSCF as a cathode in anode-supported cell with NiO-SDC and SDC as anode and electrolyte, respectively. The anode supported cell has reached the peak power densities as  $1010$  and  $402 \text{ mW}/\text{cm}^2$  at  $600$  and  $500^\circ\text{C}$ , respectively [59]. The ASR of BSCF is found in the range of  $0.055$ - $0.071 \text{ }\Omega\cdot\text{cm}^2$  at  $600^\circ\text{C}$  and  $0.51$ - $0.61 \text{ }\Omega\cdot\text{cm}^2$  at  $500^\circ\text{C}$ . These values are importantly less than other perovskite types, under relatively close conditions. The thermal expansion coefficient of BSCF is significantly high ( $20 \times 10^{-6} \text{ K}^{-1}$  at  $50$ - $1000^\circ\text{C}$ ), even though the electrochemical performance of this cathode is extraordinary, as it is usual with Co-based perovskites. Resulting that the thermal cycling process may be negatively affected because of the high thermal expansion coefficient, BSCF could mismatch with the other cell components. To overcome this problem, it is possible to use a composite cathode. Nevertheless, the use of the composite cathode may reduce the performance of BSCF.

Perovskite type nickelate  $\text{LaNiO}_{3-\delta}$  is stable at lower than  $1230$ - $1270\text{K}$ , under atmospheric oxygen pressure. Additional heating to elevated temperatures causes

decomposition of  $\text{La}_2\text{NiO}_{4-\delta}$  and  $\text{NiO}$  by the separation of  $\text{La}_4\text{Ni}_3\text{O}_{10-\delta}$  and  $\text{La}_3\text{Ni}_2\text{O}_{7-\delta}$  phases in intermediate stages [61,62]. The modifications restrict the conventional use of  $\text{LaNiO}_{3-\delta}$  based cathodes. This materials could be partially inhibited by doping in the nickel sub lattice [57]. Iron-doped nickelate exhibits phase stability in atmospheric condition.. Komatsu et al. [64,65], studied  $\text{LaNi}_{0.6}\text{Fe}_{0.4}\text{O}_3$  for IT-SOFCs as a cathode material. This material has found to have many appealing properties like high electrical conductivity (580 S/cm at 800°C) [58], high catalytic activity, and reduced mismatch of thermal expansion with the electrolyte material (zirconia). Moreover, LNF is less susceptible to poisoning from metallic components by volatile chromium species [66,67]. With the value of thermal expansion coefficient of  $11.4 \times 10^{-6} \text{ K}^{-1}$  this material's TEC value is quite close to that of 8YSZ ( $10.5 \times 10^{-6} \text{ K}^{-1}$ ). Unfortunately, LNF is more reactive toward  $\text{ZrO}_2$  based electrolytes. If the temperature of sintering exceeds 1000°C, the amount of  $\text{La}_2\text{Zr}_2\text{O}_7$  formation increases rapidly. LNF cathode sintered at 1000°C combined with a NiO-SASZ ( $\text{Al}_2\text{O}_3$  stabilized  $\text{ZrO}_2$ ) reached a maximum power density of  $1.56 \text{ W/cm}^2$  at 800°C. Here the electrolyte was 10 mole %  $\text{Sc}_2\text{O}_3$  and 1 mole %  $\text{Al}_2\text{O}_3$  stabilized  $\text{ZrO}_2$  electrolyte. When the combined concentration of Ni and Sr is near 0.6, power density reached a peak value at the temperature ranges of 600-800°C [56]. The conductivity of LSNF shows temperature dependence similar to that of metals when Sr and Ni concentrations are high. Unfortunately, with temperatures around 600°C, conductivities drop drastically.

Cobalt based materials usually have greater electronic and ionic conductivity compared to other cathode materials. For this reason, cathode materials which contain cobalt, reduce the polarization resistance. Oxygen molecules have high dissociation ability in  $\text{La}_{1-x}\text{Sr}_x\text{CoO}_{3-\delta}$ , and it has an obvious electrode activity due to high oxygen diffusivity[62]. However, a great amount of cobalt addition causes exfoliation of cathode/electrolyte interface and flaws in the electrolyte [63]. By substituting an alternative cation instead of the La; such as Gd or Pr, a decrease in the ASR and TEC can be expected. The TECs decreases in  $\text{Ln}_{0.6}\text{Sr}_{0.4}\text{CoO}_{3-\delta}$  (Ln= La, Pr, Nd, Sm, and Gd) from La to Gd.

In LSC perovskite, Sr level in addition to other effects modifies the lattice volume both in LSC-113 and LSC-214.

Effect of Sr doping in lattice parameters of  $\text{La}_{(1-x)}\text{Sr}_x\text{CoO}_{3-\delta}$  (LSC-113): Sikolenko et al. [64], investigated the correlation between lattice parameter and Sr doping amount (x) for  $\text{La}_{(1-x)}\text{Sr}_x\text{CoO}_{3-\delta}$ . X-ray powder diffraction (XRD) patterns of all specimens were recorded with an FR-552 focusing camera using  $\text{CuK}\alpha_1$  radiation with germanium as an internal standard ( $a = 5.6574\text{\AA}$ ). Neutron diffraction experiments were carried out on SING neutron source in Paul Scherrer Institute. Incident neutron wavelength was  $\lambda=2.56\text{\AA}$ . Structural analysis of diffraction patterns was obtained with FullProf Rietveld analysis program. All peaks for both samples can be indexed in the hexagonal R-3c space group. Refined parameters are listed in *Table 2.1*.

Table 2.1. *Structural parameters for  $\text{La}_{(1-x)}\text{Sr}_x\text{CoO}_{3-\delta}$  at  $x=0.15$  and  $0.3$  obtained with X-ray diffractometer by Sikolenko et al. [64], and  $x=0.5$  with neutron diffraction by Das et al. [65]*

<b>x</b>	<b>0.15</b>	<b>0.30</b>	<b>0.5</b>
<b>a (Å°)</b>	5.4493	5.4402	5.427
<b>c (Å°)</b>	13.1393	13.1793	13.254
<b>Volume (Å<sup>3</sup>)</b>	337.89	337.79	338.15

Das et al. [65] have investigated the neutron diffraction data of  $\text{La}_{0.5}\text{Sr}_{0.5}\text{CoO}_{3-\delta}$ . The neutron diffraction pattern has been recorded using a wavelength  $\lambda = 1.094 \text{ \AA}$ . Rietveld analysis of the complete pattern was performed using FullProf program. Structural parameters and cell parameters were determined from refinement, Table 2.1.

Effect of Sr doping in Lattice parameters of  $(\text{La}_{(1-x)}\text{Sr}_x)_2\text{CoO}_{4-\delta}$  (LSC-214): Powder X-ray diffraction (PXRD) and Rietveld analysis were employed by Andujar et. al. [66], as a function of composition(x), in order to carry out the structural characterization of  $(\text{La}_{(1-x)}\text{Sr}_x)_2\text{CoO}_{4-\delta}$  powders. These powders were synthesized by mixing stoichiometric amount of  $\text{La}_2\text{O}_3$ ,  $\text{SrCO}_3$  and  $\text{Co}(\text{NO}_3)_2 \cdot 6\text{H}_2\text{O}$  in nitric acid. Then, the

solution is heated to evaporate the solvent.  $\text{KNO}_3$  is added to the resulting mixture with the same mole as  $\text{Co}(\text{NO}_3)_2 \cdot 6\text{H}_2\text{O}$ . A heat treatment is employed such that the mixture was heated to  $450^\circ\text{C}$  for 1h followed by heating to  $650^\circ\text{C}$  for 48 h. Obtained product was ground and annealed at  $900^\circ\text{C}$  for 24 hr. Thereafter, it is ground again and pressed into pellets. The final heat treatment is done at  $975^\circ\text{C}$  for 24 h.

Siemens D-5000 diffractometer is used with  $\text{Cu-K}\alpha$  radiation and the data collected between  $20$  and  $80^\circ 2\theta$ , in 12 h with a step size of 0.015. Rietica program was employed for the Rietveld analysis in order to determine the lattice parameters with high precision. Results showed that the single phase  $(\text{La}_{(1-x)}\text{Sr}_x)_2\text{CoO}_{4-\delta}$  powders are obtained where the value “x” is between 0.5 and 0.7, Table 2.2.

Table 2.2. Structural parameter for of  $(\text{La}_{(1-x)}\text{Sr}_x)_2\text{CoO}_{4-\delta}$  with  $0.5 \leq x \leq 0.7$  by Andujar et al. [66] and  $(\text{La}_{(1-x)}\text{Sr}_x)_2\text{CoO}_{4-\delta}$  with  $0.375 \leq x \leq 0.75$  by James et al. [67]

<b>x</b>	<b>0.375</b>	<b>0.5</b>	<b>0.5</b>	<b>0.55</b>	<b>0.6</b>	<b>0.625</b>	<b>0.65</b>	<b>0.7</b>	<b>0.75</b>
<b>Ref</b>	[71]	[71]	[70]	[70]	[70]	[71]	[70]	[70]	[71]
<b>a (Å)</b>	3.8232	3.8073	3.8052	3.8023	3.8005	3.8001	3.8003	3.8002	3.7978
<b>c (Å)</b>	12.4992	12.5073	12.4892	12.5112	12.5212	12.5503	12.5203	12.5233	12.5162
<b>V(Å<sup>3</sup>)</b>	182.70	181.30	180.84	180.88	180.84	181.24	180.82	180.84	180.61

James et al. [67], investigated the Sr doping effect on lattice parameters of  $(\text{La}_{(1-x)}\text{Sr}_x)_2\text{CoO}_{4+\delta}$ . Polycrystalline samples of  $(\text{La}_{(1-x)}\text{Sr}_x)_2\text{CoO}_{4+\delta}$  were arranged from spectroscopic grade powders of  $\text{SrCO}_3$  (98+ %),  $\text{Co}(\text{NO}_3)_2 \cdot 6\text{H}_2\text{O}$  (98 %) and  $\text{Ln}_2\text{O}_3$  ( $\geq 99.9$  %). Dissolving the powders in dilute nitric acid leads to decomposition of citric acid- ethylene glycol sol-gel and by this way, the intimate mixture of metal oxides was formed. Then, by using tube furnace which was at  $1100^\circ\text{C}$ , the residues were pelleted and sintered under oxygen environment at most 3 days. In order to finish this reaction, this procedure was done with middle level regrinding and re-pelleting until no evidence of reaction left in powder X-ray diffraction. After that, cooling of the samples from  $1100^\circ\text{C}$  to room temperature is carried out at a rate of  $2^\circ\text{C}/\text{min}$ .

Scintag Inc XGEN 400 X-ray diffractometer was used for powder X-ray diffraction. Diffractometer which has flat plate sample holder works at ambient temperature by using  $\text{CuK}\alpha$  radiation. The adequate data were collected, between  $10$ - $110^\circ$ , with a step size of  $0.02^\circ$ , with  $10\text{s}$  collecting per step. In order to do structure refinement, rietveld method is carried out with data collected from diffractometer by using the RIETICA program [68].

Structure refinement was done for each composition of the  $(\text{La}_{(1-x)}\text{Sr}_x)_2\text{CoO}_{4+\delta}$  according to the tetragonal ( $I4/mmm$ ) structure. The results of rietveld refinement which is done by using X-ray powder diffraction data reveals that  $\text{Sr}^{+2}$  and  $\text{La}^{+3}$  ions shows disordered characteristic over the same lattice sites. A list of refined structural parameters for  $(\text{La}_{(1-x)}\text{Sr}_x)_2\text{CoO}_{4+\delta}$  compounds as determined by James et al. [67] are tabulated in Table 2.2.

#### **2.2.2.2. Composite Cathodes**

The use of composite cathode is gaining importance in recent years.  $\text{La}_{0.8}\text{Sr}_{0.2}\text{Co}_{0.5}\text{Fe}_{0.5}\text{O}_3$  (LSCF) and YSZ composite cathode commonly used, since their electrochemical activity is high and the structure remains stable at high operating temperature range. LSCF and YSZ composite cathode was fabricated by using wet impregnation method. LSCF solution is impregnated into YSZ, then the structure is pre-sintered. The study shows that the LSCF nanostructure is formed at  $700^\circ\text{C}$ . They supply large triple phase boundary for the ORR. The polarization resistance of electrode is  $0.539 \Omega\cdot\text{cm}^2$  at  $600^\circ\text{C}$  for the ORR, and  $0.047 \Omega\cdot\text{cm}^2$  for  $750^\circ\text{C}$  [69].

Ko et al. [70], investigated the LSCF-YSZ-GDC composite cathode to obtain better results in the means of cathodic performance, comparing it with LSM/GDC-YSZ. Polymerizable complex method has been used to synthesize LSCF, YSZ, and GDC. This method avoids the solid solution formation of YSZ-GDC. The electrochemical performance of LSCF/YSZ-GDC superior than LSCF-GDC cathode at  $800^\circ\text{C}$ . The polarization resistance of LSCF/YSZ-GDC cathode was  $0.075 \Omega\cdot\text{cm}^2$ , which was significantly lower than that of LSCF-GDC cathode ( $0.195 \Omega\cdot\text{cm}^2$ ).

LSCF-GDC composite cathode was studied by Leng et al. [71] with GDC electrolyte. Pure LSCF has polarization resistance as  $1.20 \Omega \cdot \text{cm}^2$  at  $600^\circ\text{C}$ . Glycine-nitrate combustion method was used to synthesize LSCF. When GDC is added to LSCF, the polarization resistance was reduced to  $0.17 \Omega \cdot \text{cm}^2$  at  $600^\circ\text{C}$ . For low temperature SOFCs, the LSCF-GDC composite cathode, therefore showed promising results.

Murray et al. [72], have investigated the LSM-GDC and LSM-YSZ composite cathodes in terms of electrochemical performance. LSM-GDC composite cathode has superior properties compared to LSM-YSZ cathode, as GDC have higher ionic conductivity than YSZ, and does not react with LSM. The results showed that GDC addition to the LSM decreased the cathode resistance approximately seven times.

LSC-113 and LSC-214 has attracted considerable attention in recent years as composite cathode [6]. This belongs to the so-called MIEC oxides with exceptionally high ORR made possible with the presence of hetero interface. Since this system is of particular relevance to the current work, the synthesis of LSC113-LSC214 composite cathodes are described below in a greater detail.

### **2.3. Synthesis of Composite Cathode**

Among cathode materials, LSC has gained remarkable interest with its superior ORR at comparatively low temperatures. Recently, it has been proven that when the LSC-113 is mixed with the Ruddlesden-Popper type cobaltite (LSC-214), the kinetics of cathode can be improved drastically. Feng et al.[73], found that ORR kinetics were significantly increased with these mixed oxides. This increase was connected with the positive effects of hetero-interface in the composite cathode [53]. Hence, efforts have focused on LSC based composite cathodes interface maximizing.

Sase et al. [53], discovered in LSC-214 phase which was formed accidentally as a result of over sintering of  $(\text{La}_{0.6}\text{Sr}_{0.4})\text{CoO}_{3-\delta}$  at elevated temperatures. In this study hetero-interface was observed by secondary ion mass spectroscopy (SIMS). The electrical conductivity of the composite was significantly higher than that of  $(\text{La}_{0.6}\text{Sr}_{0.4})\text{CoO}_{3-\delta}$  at the same temperature.

Recently Sase et al. [53] have reported enhanced ORR kinetics of  $\sim 3$  orders of magnitude at the interfaces between bulk  $(\text{La}_{0.6}\text{Sr}_{0.4})\text{CoO}_{3-\delta}$  (LSC-113) grains and secondary  $(\text{La,Sr})_2\text{CoO}_{4\pm\delta}$  precipitates relative to bulk LSC-113. Subsequently these authors show that  $\sim 1$  order of magnitude enhancement in ORR activity can be obtained for composite cathodes screen-printed with these two oxide materials [74]. For further clarification, Crumlin et al. [3] obtained epitaxial thin film cathodes by pulsed layer deposition (PLD). They deposited LSC-214 on LSC-113 with both full and partial coverage. They, revealed that the active region is affected by TPB (LSC113-gas-LSC214) which has around 20  $\mu\text{m}$  thickness of cathode. Thus the ASR gets dramatically increased, when the thickness of deposited LSC-214 on LSC-113 increase. In this sense, what Sase et al. [53] found first is corrected by Crumlin et al.[75], who detected, 3-4 orders of magnitude enhancement in  $k^a$ . Hence, they recorded the effect of hetero interface in overall resistance, rather than recording the enhancement just at interface, which was at most one order of magnitude consistently [74].

Muturo et al., [76] have investigated the multi-layer approach where LSC-214 cover completely the LSC-113, the main phase. Also, they have used the surface decoration technique. To maximize the interfacial region, the individual columns with a width of 100-500 nm have deposited as vertically aligned columns [5]. In these studies, the volume fractions of LSC-214 were in between 0.10 to 0.35,. They reported an ASR value of  $1000 \Omega \cdot \text{cm}^2$  at  $400^\circ\text{C}$  in this composite with vertical columns. This ASR value is 10 times smaller than ASR of single phase cathodes at similar temperatures. The temperature of  $400^\circ\text{C}$  was important as this is a critical threshold above which surface Sr segregation did occur in the composite cathode. Another interesting observation was that, hetero-interface has a capability to delay chemical degradation of the cathode surface [77].

In another approach Sari et al. [6], used the co-sputtering technique which was utilized due to the apparent advantage of hetero interfaces, in order to improve cathode performance at intermediate temperatures. They investigated the effect of varying

the phase fractions on cathode performance. The most suitable compositions were found to be LSC-113, LSC-214=0.45:0.55. When  $ASR=0.15 \Omega.cm^2$  was taken as a benchmark, this composition would allow the use of cathode as low as  $575^\circ C$ .



## CHAPTER 3

### EXPERIMENTAL PROCEDURE

This chapter comprises materials and methods used in the current work. First synthesis of LSC powders via thermal plasma are described. Then, methods used in electrochemical and materials characterization are given.

#### 3.1. LSC Composite Powder Synthesis via Radio Frequency Thermal Plasma

Precursors used for the synthesis of LSC113-LSC214 powders were nitrates, namely  $\text{La}(\text{NO}_3)_3 \cdot 6\text{H}_2\text{O}$  (Alfa Aesar, 99.99%),  $\text{Sr}(\text{NO}_3)_2$  (Alfa Aesar, 99.0%) and  $\text{Co}(\text{NO}_3)_2 \cdot 6\text{H}_2\text{O}$  (Alfa Aesar, 98-102%).

Powder synthesis was carried out with a 30 kW thermal induction plasma. A schematic representation of the plasma system is given in Figure 3.1. The system consists of an RF power supply (30 kW), a plasma torch and powder collectors.

At the top of the reactor the plasma torch is placed, Figure 3.2. Plasma is formed in the central portion of the torch via induction coupling using Ar as plasma gas. Precursors are sent to the injection probes, where they reach and penetrate into the plasma. The temperature could be reach as high as  $T > 10000^\circ\text{C}$  at the plasma region. The precursors injected are later vaporized and immediately condensed in the quenching zone where normally nitrogen is used with a high rate as a quenching medium.

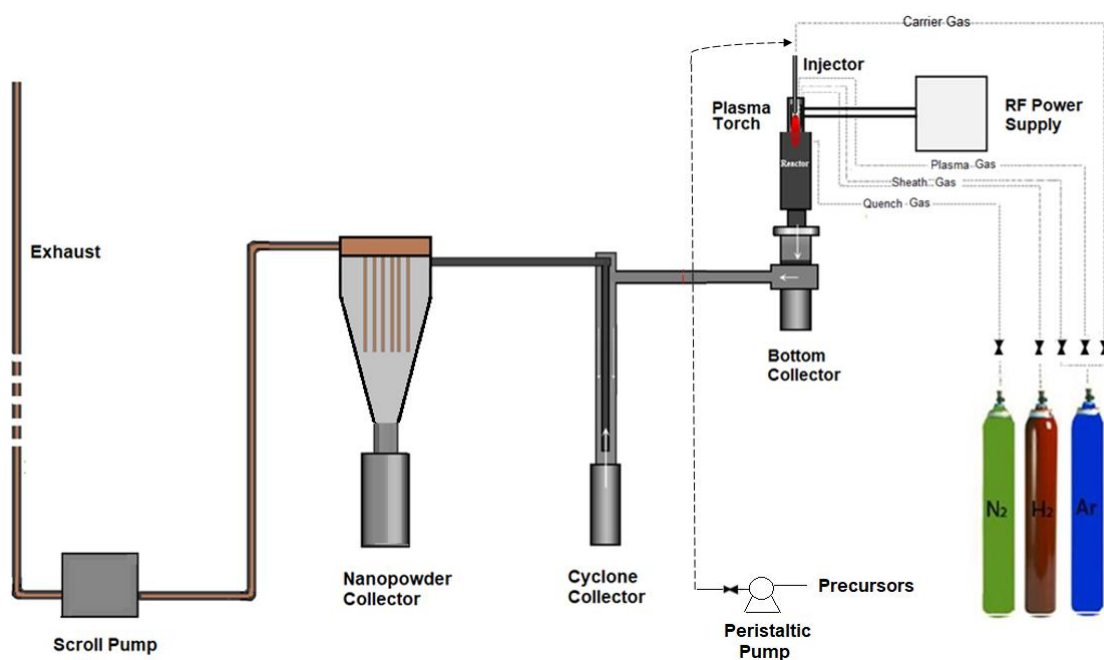


Figure 3.1. Schematic illustration of the induction plasma system.

During processes, the plate power kept constant at approximately 25 kW when induction plasma torch is operated. Plasma forming gas, which called as central gas, was used as pure argon (Linde, 99.995% purity). The central gas was sent through the inner quartz tube into the torch, with a flow rate of 15 slpm. Sheath gas was used as a combination of pure argon (Linde, 99.995% purity) and pure hydrogen (Linde, 99.995% purity), which is sent through the space between the inner tube and the outer confinement tube. Argon was procured at 60 slpm, then plasma is ignited. Subsequently, hydrogen in the sheath gas was increased differentially to 6 slpm. Since sudden increment of hydrogen could extinguish the plasma, the gradual increase is required, especially at the low plasma power. In addition to argon, hydrogen is also added to provide more effective protection of confinement tube from excessive heat.

Since plasma ignition is much easier at low pressure, the starting pressure was kept nearly 0.28 bar in all experiments. After that, the hydrogen flow, power and the pressure were increased in turn. The power was ensured slowly to the set power (25 kW). The pressure was increased to 0.48 bar, and the hydrogen flow was also

increased to the 6 slpm. Finally, the torch pressure obtained approximately 0.97 bar, which is less than the atmospheric pressure, in all experiments.

Precursors are fed into the torch from the top injector. The precursors can be solid, liquid and gas to be fed through the injector. In the current experiments, the precursor solution prepared was fed into the torch at a rate of 10 mL/min by a peristaltic pump. Carrier gas was used as Ar (Linde, 99.995% purity), and fed at 4 slpm.

Injector used as a solution atomizer. This enables atomization of the solution just above the plume with the use of argon maintained at a flow rate of 5 slpm. The position of the atomization probe and the flow rate of the precursors are adjusted according to the optimum dispersion of the precursors. The reactor also incorporates a quenching zone. For this aim, nitrogen gas was used with flow rate of 150 slpm.

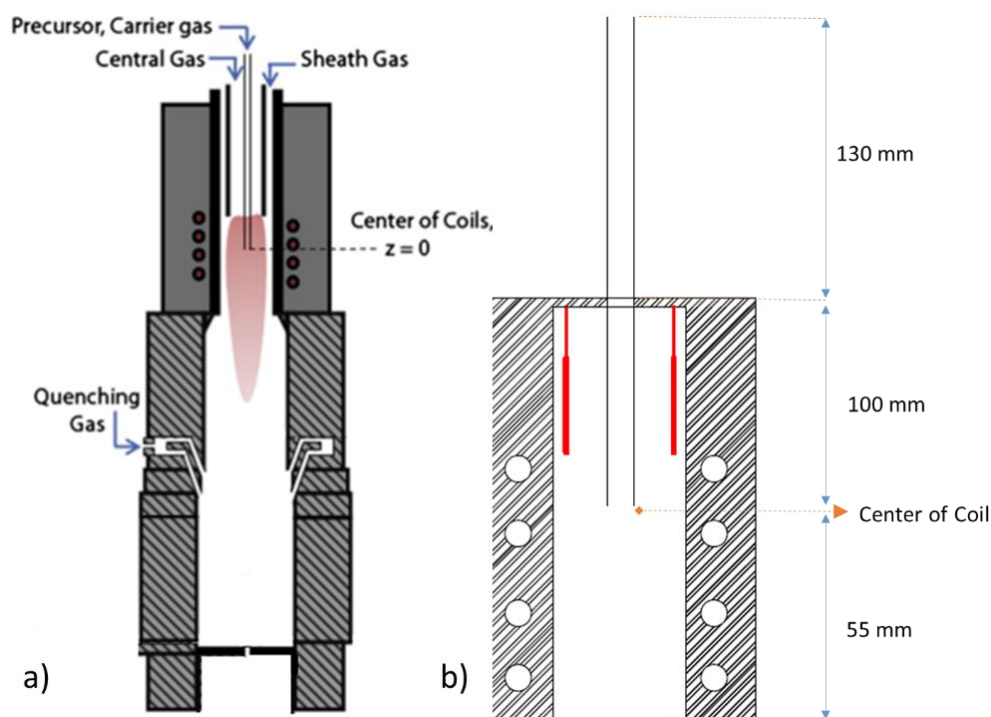


Figure 3.2. Schematic diagram of, a) the induction plasma torch, and b) the location of atomization probe.

Powders synthesized are collected from the bottom, cyclone and nanopowder collectors according to their size ranges. Large particles are collected in the bottom collector and cyclone collector where the flue gas makes a 90° turn and a 180° turn, respectively. Particles collected in nanopowder collector are typically less than 100 nm in size.

### 3.2. Material Characterization

Powders synthesized by the thermal plasma system were characterized by X-ray diffraction, scanning electron microscopy (SEM) and transmission electron microscopy (TEM). X-ray analysis were carried out using D/MAX-2200 Rigaku X-ray Diffractometer with Cu-K $\alpha$  radiation, with 0.02°/min scan rate. Where necessary, the X-ray pattern were refined by Rietveld refinement technique using Maud software [78]. Morphologies of the powders are investigated by using field emission scanning electron microscope, FEI Nova NanoSEM 430. For this purpose, samples were attached to the aluminum stub holders via double sided conductive carbon tape. Where needed particles in SEM were examined using EDX analysis so as to determine their composition. Synthesized powders were examined with high resolution transmission electron microscope (Jeol 2100F HRTEM). Samples for TEM were prepared, by adding small amount of powder to ethanol and ultra-sonicated for 5 minutes. Then a small droplet was applied with a pipet to holy carbon grid.

Specific surface area of the powders was obtained via multi-point measurement BET (Brunauer, Emmett and Teller) analysis using Quantachrome Corporation (Autosorb-1C/MS).

Average particle diameter was derived from this value by Equation 3.1 (assuming all the particles are spherical in shape).

$$d_{BET} = \frac{6}{(S_{BET} \times d)} \quad \text{Eq. 3.1}$$

Where  $d_{BET}$  is the average diameter of the particles,  $S_{BET}$  is the specific surface area value obtained from the analysis and  $d$  is the density of the material.

### 3.3. Fabrication of Symmetric Cell

A symmetric cell is formed from three layers, cathode on the either side and the electrolyte in between, Figure 3.3. The cathode slurries were screen-printed onto both side of the electrolyte.

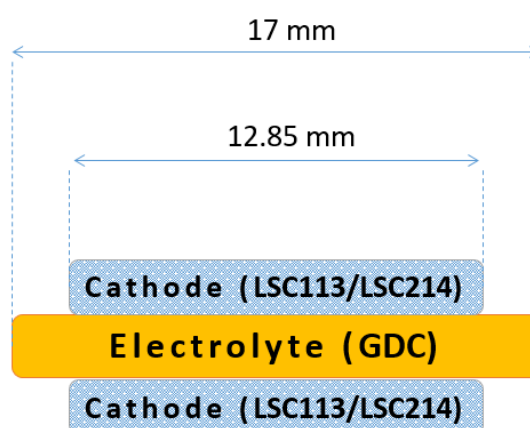


Figure 3.3. Schematic drawing of symmetric cell in cross-sectional view.

The electrolyte was GDC pellet 17 mm in diameter with 1 mm in thickness. For this purpose, GDC powders were pressed into 19-mm diameter pellets which was sintered at 1350°C for 10 hours.

There are several approaches in preparation of screen-printing slurry. Somalu et al. [79], examined the slurry behavior by comparing the solvents; the anhydrous terpineol and texanol. The binder and dispersant was fixed as ethyl cellulose N7 grade and hypermer KD15, respectively. Based on the study, the solvent type has not significant effect on the slurry. According to Ried et al. [80], the pastes produced, contained terpineol as a solvent, polyvinylpyrrolidon (PVP) as a dispersant and polyvinylbutyral (PVB) as a binder. Optimal printing results were obtained using pastes with PVB as a binder and resulted in gas tight layers.

Cathodes on either side were LSC-113/LSC-214 composite. These were screen printed using ink prepared by composite powder with solvent binder and dispersants.

In this study, texanol was used as solvent, hydroxyethyl cellulose as a binder, 0.15 wt.% and the polyvinylpyrrolidon (PVP) 5 wt.% as dispersant. The function of dispersant is to improve the separation of solid particles by the formation of an electrostatic or a steric barrier around the particle surfaces, so that the interparticle forces between neighboring particles can be optimized to a satisfactory level, and consequently reduce the viscosity and elastic modulus of an ink. In addition, the addition of dispersant may stabilize the ink by preventing particle agglomeration over time. The longer the hydrocarbon chains, the better the stabilization effect [81]. Screen printing was achieved using a 195 mesh screen, Figure 3.4.



*Figure 3.4.* Digital image of the screen-printing device.

### **3.4. Electrochemical Characterization**

For electrochemical characterization, gold contacts were established on the symmetric cells, Figure 3.5. The gold contact was formed with a gold paste (8884-G ESL Europe) in an area of 10.75 mm diameter which was printed on the cathode 12.85 mm in diameter. In this way, 0.389 cm<sup>2</sup> uncoated cathode area has obtained, which exposed to the atmosphere. The gold wires were used as connections, in the gold layer.

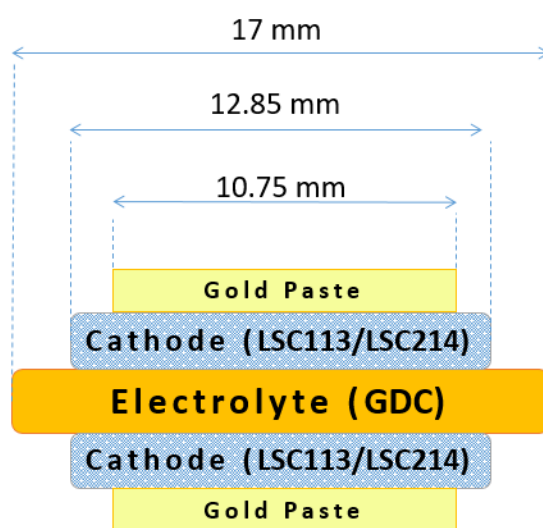


*Figure 3.5.* Schematic representation of symmetric cell used in electrochemical impedance spectroscopy.

The symmetric cell was established to one end of an alumina tube 14 mm in inner and 25 mm in outer diameter. The cell placed at one end of the tube was sealed with the use of ceramic sealant (AREMCO Product No: 552-1178), Figure 3.6.



*Figure 3.6.* Assembly of the symmetric cell for EIS measurements in a split furnace.

Electrochemical impedance spectra (EIS) were collected on the cell using potentiostat/galvanostat (Gamry Inst. Reference 3000) with a disturbance voltage of 10 mV from 1 MHz to 0.1 Hz. Measurements were carried out at temperatures ranging from 300-700°C. Finally, the spectrum was fitted using equivalent circuit given by Januschewsky [82].



## CHAPTER 4

### RESULTS AND DISCUSSION

LSC powder was synthesized from a precursor solutions prepared by mixing nitrates, namely  $\text{La}(\text{NO}_3)_3 \cdot 6\text{H}_2\text{O}$ ,  $\text{Sr}(\text{NO}_3)_2$  and  $\text{Co}(\text{NO}_3)_2 \cdot 6\text{H}_2\text{O}$ . For this purpose, nitrates mixed in proportions given in Table 4.1 were dissolved in excess amount of deionized water and mixed together to yield a single solution. Concentration achieved are given in Table 4.1.

The synthesis was achieved in a radio frequency (R.F.) plasma (TEKNA, 30 kW) using parameters given in Chapter 3. The precursor solution was fed into 10 ml/min. The synthesized powders collected from the filter are given, Figure 4.1.

Table 4.1. Concentrations of nitrates used for the preparation of precursor solution.

<i>Nitrates</i>	<i>Mole number (mole)</i>	<i>Concentration (g/mL)</i>
$\text{La}(\text{NO}_3)_3 \cdot 6\text{H}_2\text{O}$	0.029	0.099
$\text{Sr}(\text{NO}_3)_2$	0.029	0.709
$\text{Co}(\text{NO}_3)_2 \cdot 6\text{H}_2\text{O}$	0.029	1.338



Figure 4.1. Synthesized LSC powders by thermal plasma collected on filter.

#### 4.1. Characterization of LSC powder

Synthesized LSC powder has a fine scale structure, Figure 4.2. A macro size sample was prepared from the synthesized powder pressed into a pellet. EDS data collected at low magnification (x800), accelerating voltage of 30 kV, spot size 4.5 yielded a composition which was not too far off from that expected from precursor solution, Table 4.2. Mole fractions of nitrates used for the preparation of precursor solution given in Table 4.2 and Table 4.3.

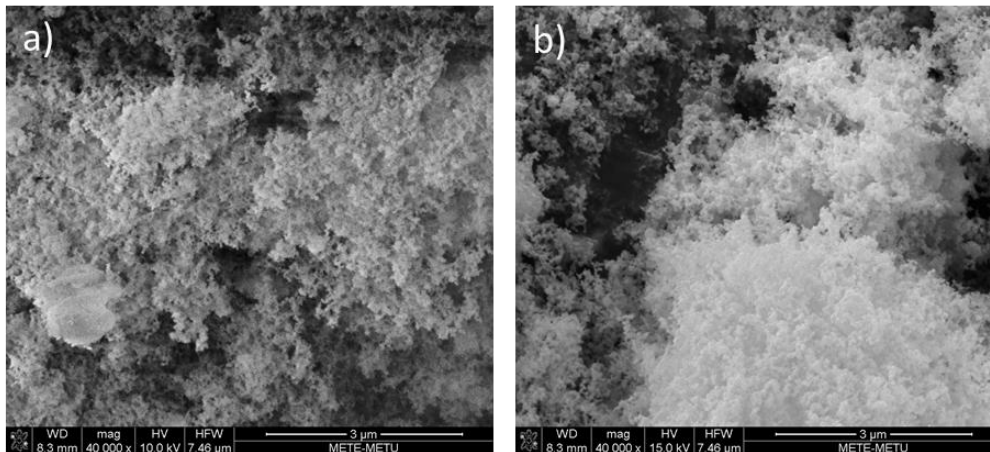


Figure 4.2. SEM image of LSC powder a) synthesized, b) annealed powder.

Table 4.2. Mole fractions of nitrates used for the preparation of precursor solution.

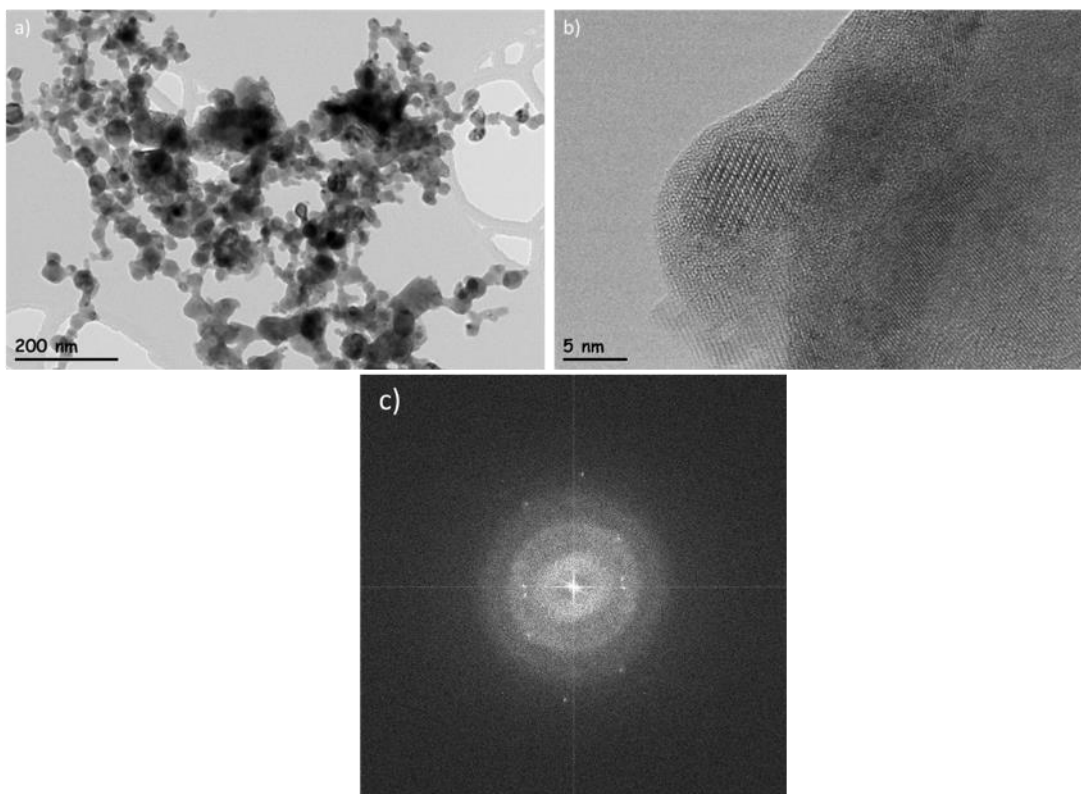
<i>Nitrates</i>	<i>Amount (g)</i>	<i>Wt. %</i>	<i>Mole number (mole)</i>	<i>Molar Ratio <math>\frac{n_i}{n_{tot}}</math></i>
La(NO <sub>3</sub> ) <sub>3</sub> .6H <sub>2</sub> O	12.557	46	0.029	33.3
Sr(NO <sub>3</sub> ) <sub>2</sub>	6.137	23	0.029	33.3
Co(NO <sub>3</sub> ) <sub>2</sub> .6H <sub>2</sub> O	8.44	31	0.029	33.3

Table 4.3. EDS results of synthesized LSC powder.

<i>Element</i>	<i>Atomic (%)</i>	<i>Weight (%)</i>
<i>La</i>	29	46
<i>Sr</i>	35	23
<i>Co</i>	36	31

BET analysis yielded a specific surface area of 15.87 m<sup>2</sup>/g for plasma synthesized powder. Assuming all the particles are spherical in shape, average particle size was calculated using the equation 3.1. Where the average density for LSC was taken as 6.5 g/cm<sup>3</sup>. This has yielded a particle size as 58.2 nm.

A typical example of TEM images of powder are given in Figure 4.3. As seen in Figure 4.3(a) particles are uniform in size yielding an average particles size of 45 nm. This value is less than what was obtained from BET analysis. Figure 4.3(b), refer to lattice imaging from a selected particle and Figure 4.3(c) shows the diffraction pattern taken from the same particle. Both imply a nanocrystalline powder.



*Figure 4.3.* TEM images of plasma synthesized LSC powder.

XRD pattern of the synthesized powder is given in, Figure 4.4. The position of peaks expected from LSC-113 and LSC-214 are indicated in the pattern. It is seen that both phases are present but there are also additional peaks.

Since thermal plasma and associated fast quenching can lead to non-equilibrium structure, the powder was annealed at 800°C for 5 hours so as to establish equilibrium in the powder. This has resulted in a decrease of surface area in BET analysis where the average particle size was now 72.6 nm, after annealing process.

Rietveld refined XRD pattern obtained after annealing is given in Figure 4.5. The pattern is similar to that recorded before annealing, but peaks are much sharper implying improved crystallinity in the annealed sample. The structural parameters

obtained with rietveld refinement are tabulated in the Table 4.4. Additional peaks are still present in the pattern.

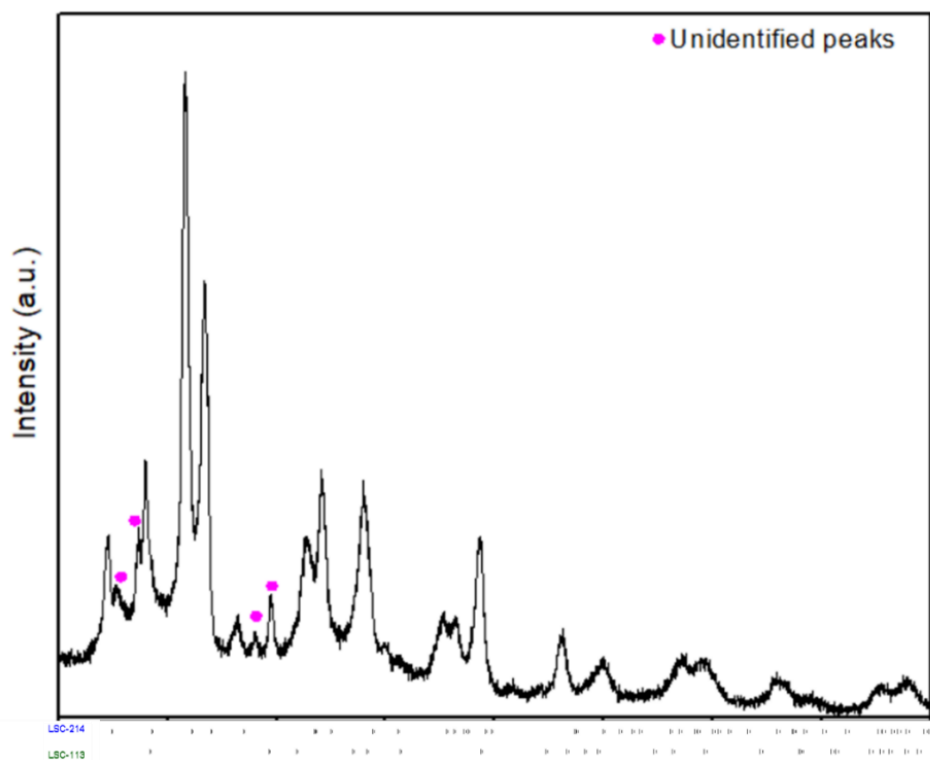


Figure 4.4. X-ray diffractogram of LSC powder synthesized by induction thermal plasma.

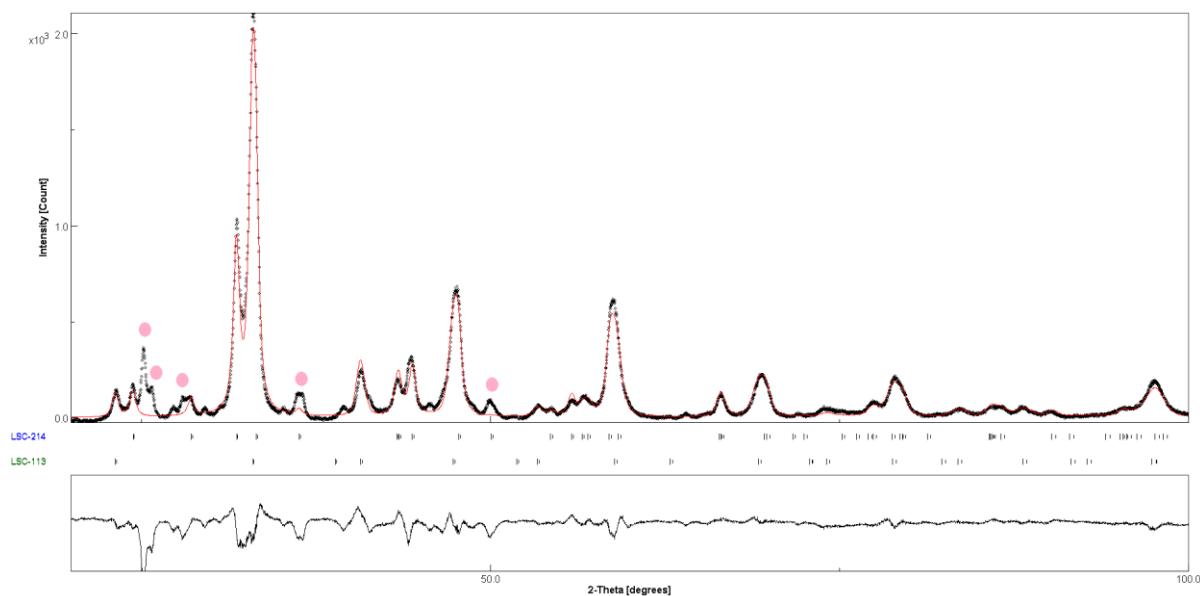


Figure 4.5. Rietveld refinement of the X-ray diffractogram of powder synthesized by induction thermal plasma after 800°C 5h annealing.

Unidentified peaks most probably belong to strontium carbonate ( $\text{SrCO}_3$ ) phase. When the synthesized powder exposed to air,  $\text{Sr}(\text{OH})_2$  phase is formed at first, which could then have transformed to  $\text{SrCO}_3$ . In order to check these assumptions, a new sample was prepared. XRD pattern of this sample is given in Figure 4.6(a) where the same unidentified peaks are observed. Figure 6(b) refers to the same sample heated to 1300°C. It should be noted that with this treatment the additional phase disappears as carbonate decomposes at this temperature[83].

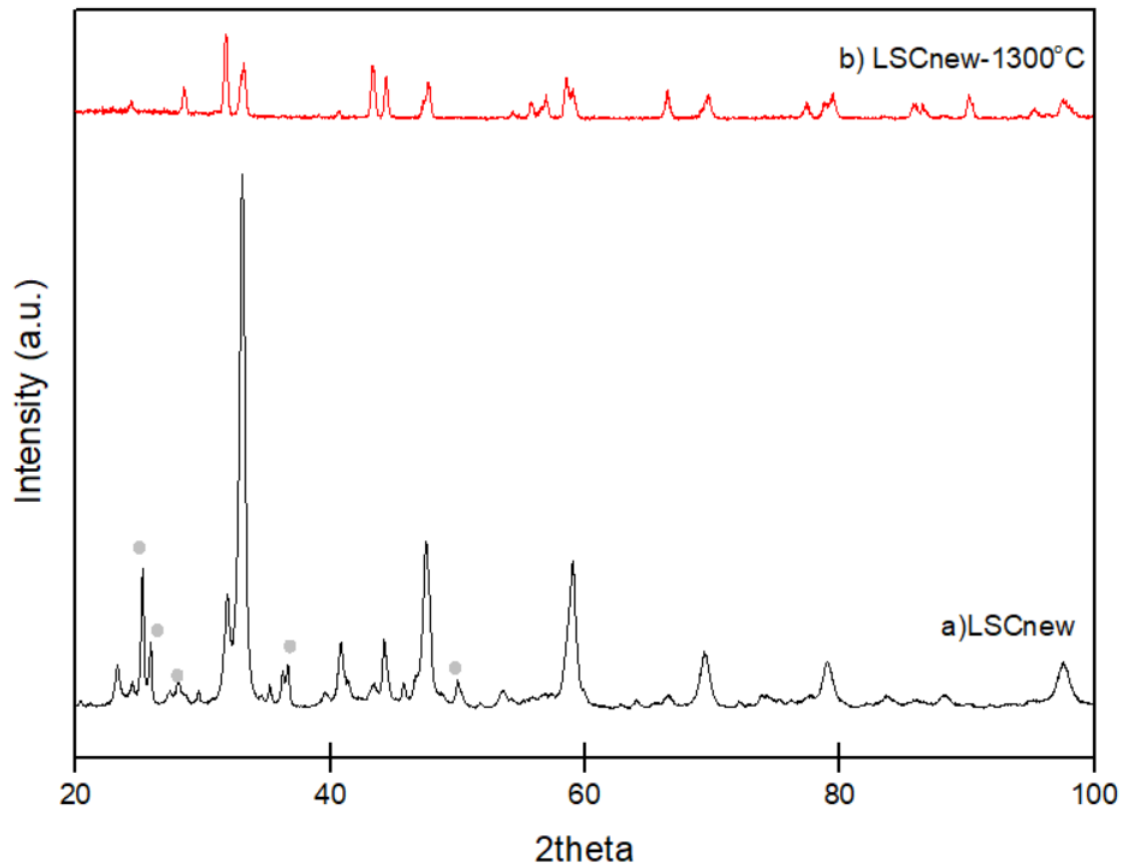


Figure 4.4. X-ray diffractogram of LSC powders a) new composite cathode, b) heated 1300°C for 1h.

Returning to the original powder, the Rietveld refinement was repeated for taking into account three phases, LSC-113, LSC-214 and  $\text{SrCO}_3$  phase, Figure 4.7. This yields the results; where LSC-113:LSC-214: $\text{SrCO}_3$ = 0.50:0.36:0.14 by weight.

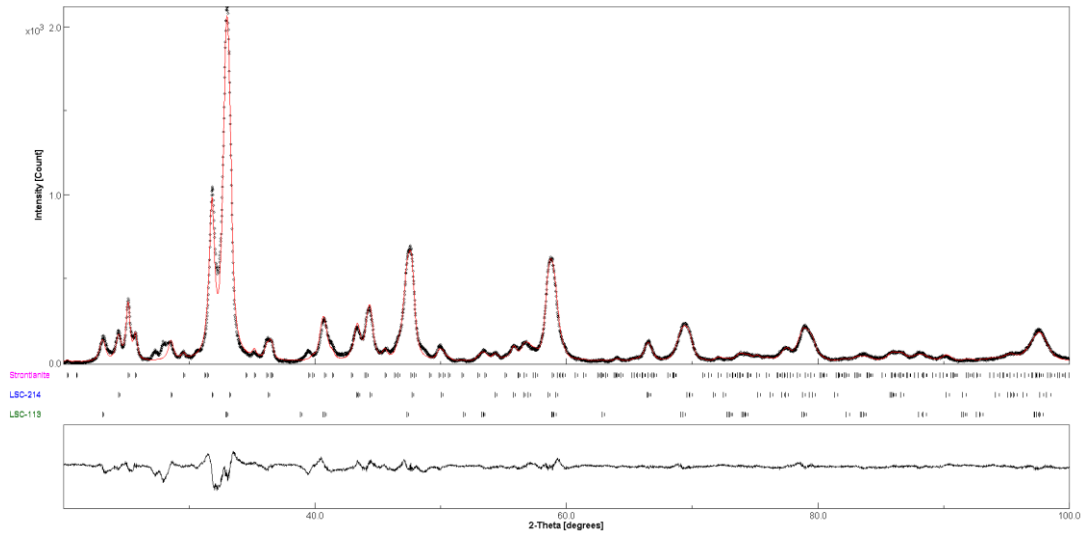


Figure 4.5. Rietveld refinement of the X-ray diffractogram of powder synthesized by thermal plasma, with SrCO<sub>3</sub> phase.

Table 4.4. Lattice parameters of refined LSC powder after annealing.

Lattice Parameters	a (Å)	b (Å)	c (Å)	V (Å <sup>3</sup> )
<b>LSC-113 (hexagonal)</b>	5.428	5.428	13.290	339.1
<b>LSC-214 (tetragonal)</b>	3.8090	3.8090	12.487	181.17

The lattice parameters of LSC-113 and LSC-214 varies with Sr occupation as given in Chapter 2. Based on the current lattice parameter Sr occupation in the present phases can be determined from this dependence. Considering first LSC-113, i.e. La<sub>(1-x)</sub>Sr<sub>x</sub>CoO<sub>3</sub>, using the lattice volume value of 339.1 Å<sup>3</sup> yields x = 0.76, as seen in Figure 4.6. Repeating the same using the lattice volume of 181.17 Å<sup>3</sup> for LSC-214 (La<sub>(1-x)</sub>Sr<sub>x</sub>)<sub>2</sub>CoO<sub>4</sub> gives x as 0.46, Figure 4.7.

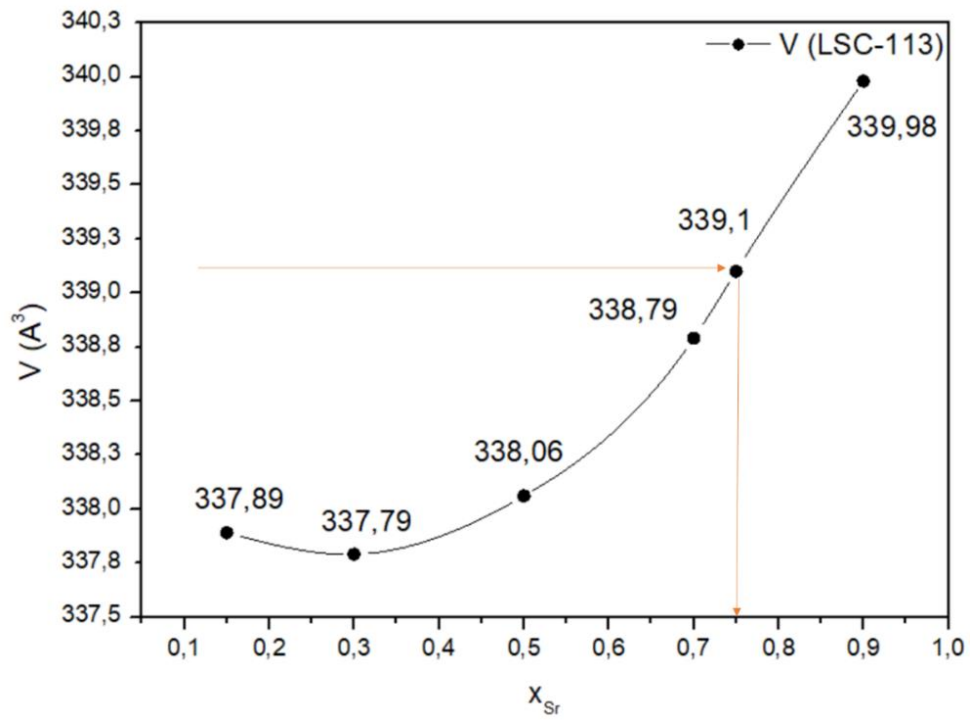


Figure 4.6. Lattice volume of LSC-113 on Sr-doping dependence [64].

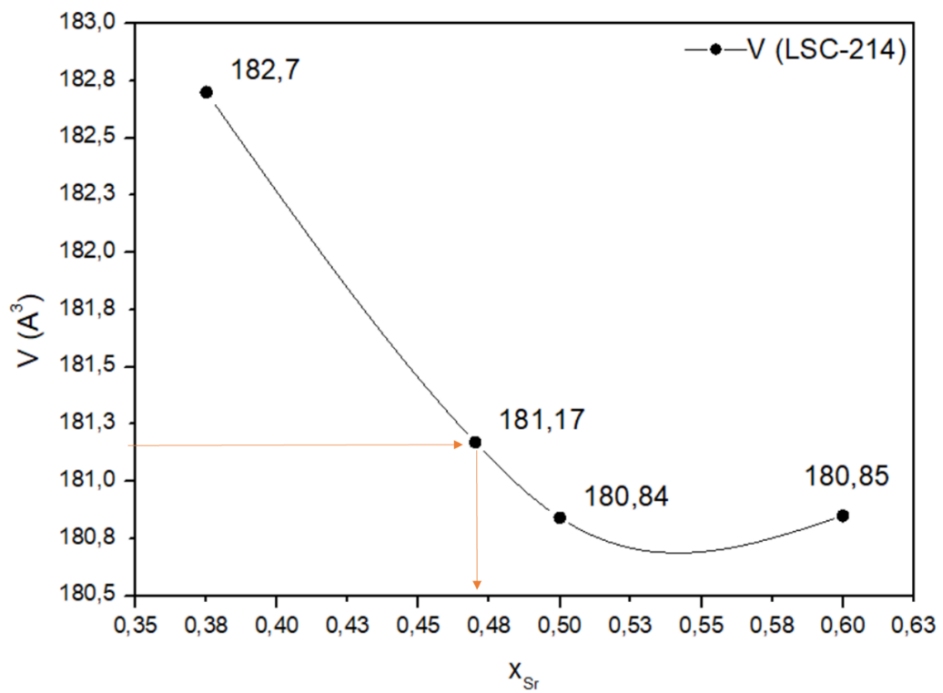


Figure 4.7. Lattice volume of LSC-214 on Sr-doping dependence [66,67]

Thus two phases making up the synthesized powders seem to have a composition of  $\text{La}_{0.24}\text{Sr}_{0.76}\text{CoO}_3$  for LSC-113 and  $(\text{La}_{0.54}\text{Sr}_{0.46})_2\text{CoO}_4$  for LSC-214.

Annealed powder has a chemical composition almost identical to that given in *Table 4.3*. Based on the compositions  $\text{La}_{0.24}\text{Sr}_{0.76}\text{CoO}_3$ , i.e. LSC-113 and  $(\text{La}_{0.54}\text{Sr}_{0.46})_2\text{CoO}_4$ , considering that La content as determined with EDS analysis has a value of 29 at. %, this yields a mixture where the molar fraction of phases is LSC-113: LSC-214= 0.3:0.7. The quantities here determined based on La, Sr and Co content has slightly difference with, what was required for the mixture LSC-113: LSC-214= 0.3:0.7.

## 4.2. Electrochemical Characterization

After assuring the structural characteristics of powders, they were used to fabricate symmetric cells. First plasma synthesized powder was tested in as-synthesized condition. For this purpose, symmetric cell was prepared by screen printing the powder on both sides of GDC electrolyte of 17-mm diameter. As seen in *Figure 4.8(a)* the cell has a total thickness of slightly more than 1 mm. *Figure 4.8 (b)* is the magnified image of the LSC composite as applied to the both surface of the cell. It is seen that the screen printed cathode has an average thickness of  $3.07\ \mu\text{m}$ . For LSC cathodes the value of critical thickness,  $L_c$ , lies in the range of 1-40  $\mu\text{m}$  in the temperature range of 400-700°C [76,88,89].

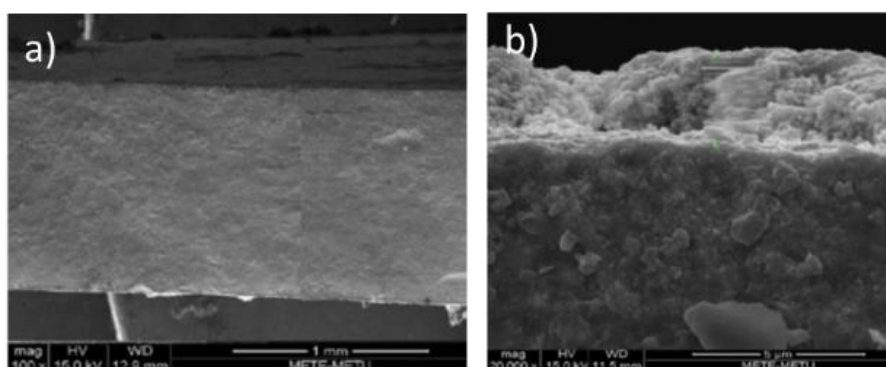


*Figure 4.8.* Cross sections of the symmetric cells produced with synthesized powder a) the complete cross-section b) The magnified image of LSC electrode applied to the surface.

Symmetric cells fabricated with screen-printing of LSC-113 and LSC-214 were analyzed according to their electrochemical impedance spectrum (EIS). Measurements were carried out at constant temperatures in the range of 350-700°C with 50°C intervals. The typical EIS response for 350-500-700°C temperatures are given in Figure 4.9.

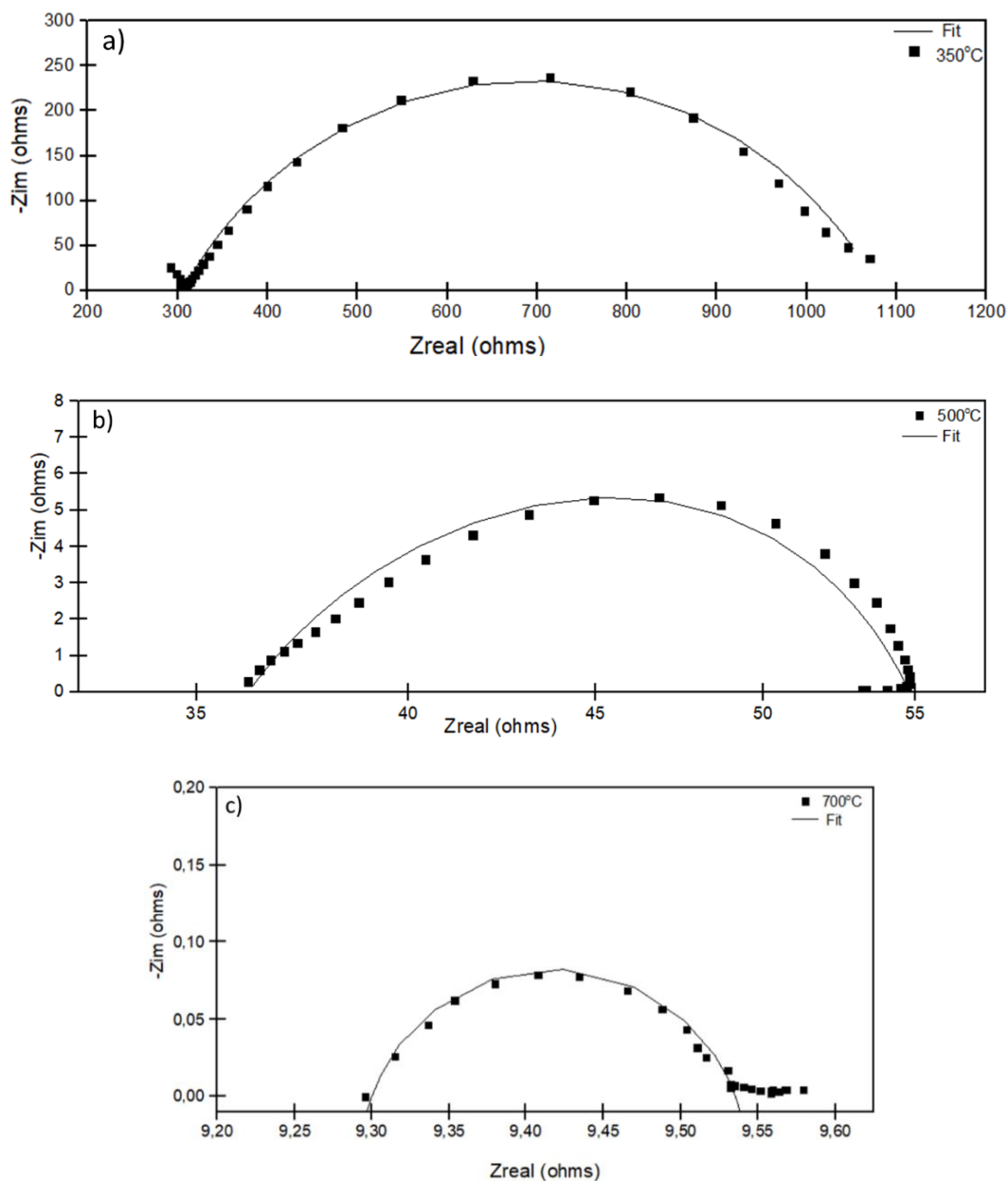


Figure 4.9. Illustration of an EIS example observed in screen-printed symmetric cells for a)350, b)500, and c)700 °C.

As it can be seen in Figure 4.9(b), the low frequency arc was almost complete by intersecting the x-axis at about  $Z_{\text{real}} = 55$  ohms. The total  $R_{\text{cathode}}$  value of 19 ohms was extracted from the model as shown on the figure.  $\text{ASR}_{\text{cathode}}$  was obtained by multiplying  $R_{\text{cathode}}$  with the active cathode area ( $0.39 \text{ cm}^2$ ) and dividing it by 2 (due to the use of symmetric cells). The value of  $\text{ASR}_{\text{cathode}}$  corresponding to this spectrum for example was  $3.50 \text{ ohm.cm}^2$ .

Table 4.5. The cathode resistance and ASR values of LSC-113: LSC-214 in various temperatures.

T (°C)	$Z_{\text{real}}$	$R_{\text{cathode}}$ (ohms)	ASR (ohms*cm <sup>2</sup> )
350	330	1068	143.54
400	137	293	30.34
450	63	109	8.95
500	36	54	3.5
550	22	31	1.75
600	15	18	0.58
650	11	12	0.195
700	9.30	9.54	0.0468

The cathode resistance and area specific resistance of composite cathodes in 350-700 °C temperatures interval are given in *Table 4.4*. These values are shown plotted in form of  $\log(\text{ASR})$  vs  $1000/T$  for each temperature at atmospheric condition and oxygen is added, Figure 4.10. According to Figure 4.10, the  $\log(\text{ASR})$  values are decreasing with temperature as expected. Good linearity of the cathode ASR versus reciprocal temperature was observed. The activation energy of the cathode is calculated as 120.62 kJ/mole.

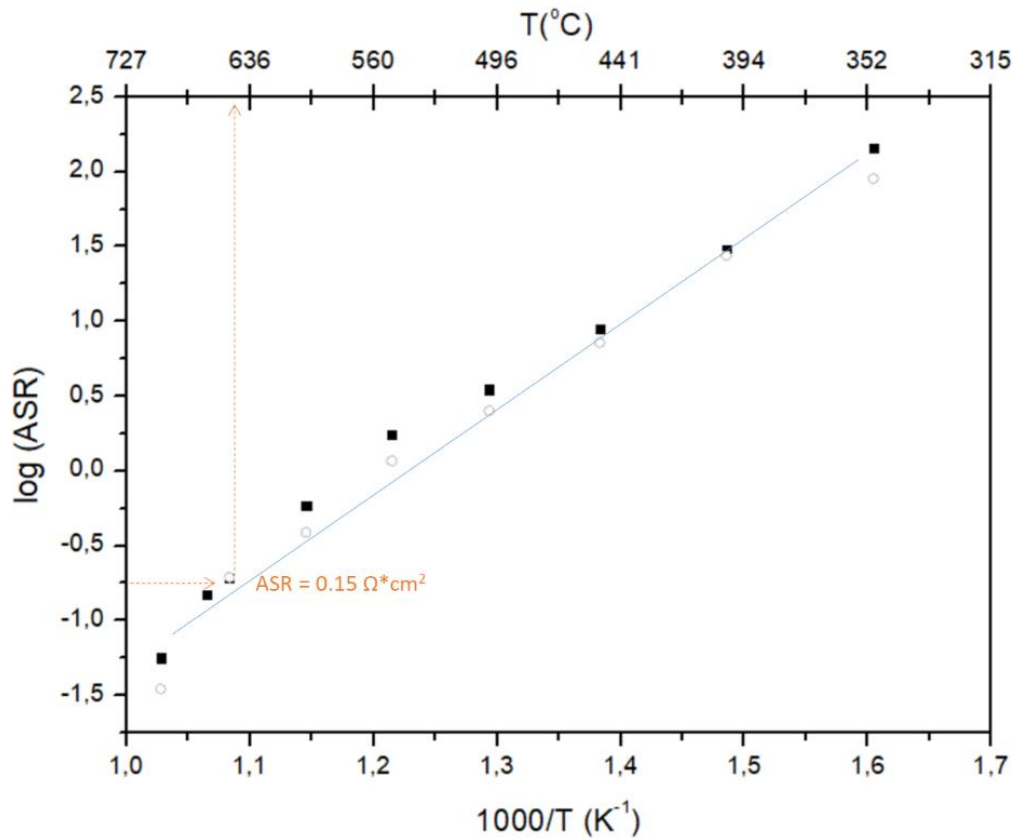


Figure 4.10. The relationship between the  $\log(\text{ASR})$  vs  $1000/T$  [ $\text{K}^{-1}$ ] for LSC-113/LSC-214 composite cathode. The ASR values with  $\text{P}_{\text{O}_2}$  is also added for comparison. The solid points represent composite cathode under atmospheric condition and the hollow points represent the oxygen rich atmosphere.

For practical application of SOFC, ASR value of  $0.15 \Omega \cdot \text{cm}^2$  provides useful benchmark. This value is marked in Figure 4.10. It is seen that the corresponding temperature is  $665^\circ\text{C}$ . This implies that the cathode can be used at operating temperature  $T_{\text{op}} \geq 665^\circ\text{C}$ . Sari et al. [6], reports  $T_{\text{op}}$  of  $700^\circ\text{C}$  for the similar composition of cathode produced by sputter deposition. In his study, the activation energy of the LSC-113: LSC-214 composite cathode is calculated as  $172.50 \text{ kJ/mole}$  according to slope of the  $\log(\text{ASR})$  vs  $1000/T$  graph. Since, the activation energy of the plasma synthesized sample is similar with the sputtered ones, the temperature obtained for the targeted ASR ( $\sim 0.15 \text{ ohm} \cdot \text{cm}^2$ ) is also related.

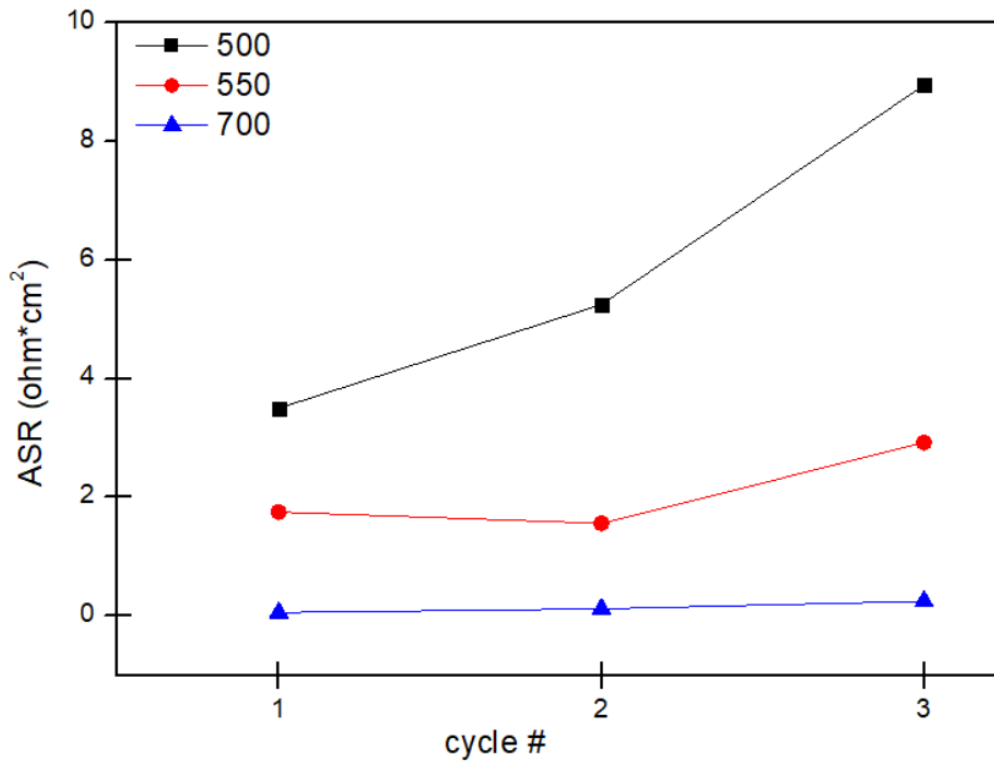
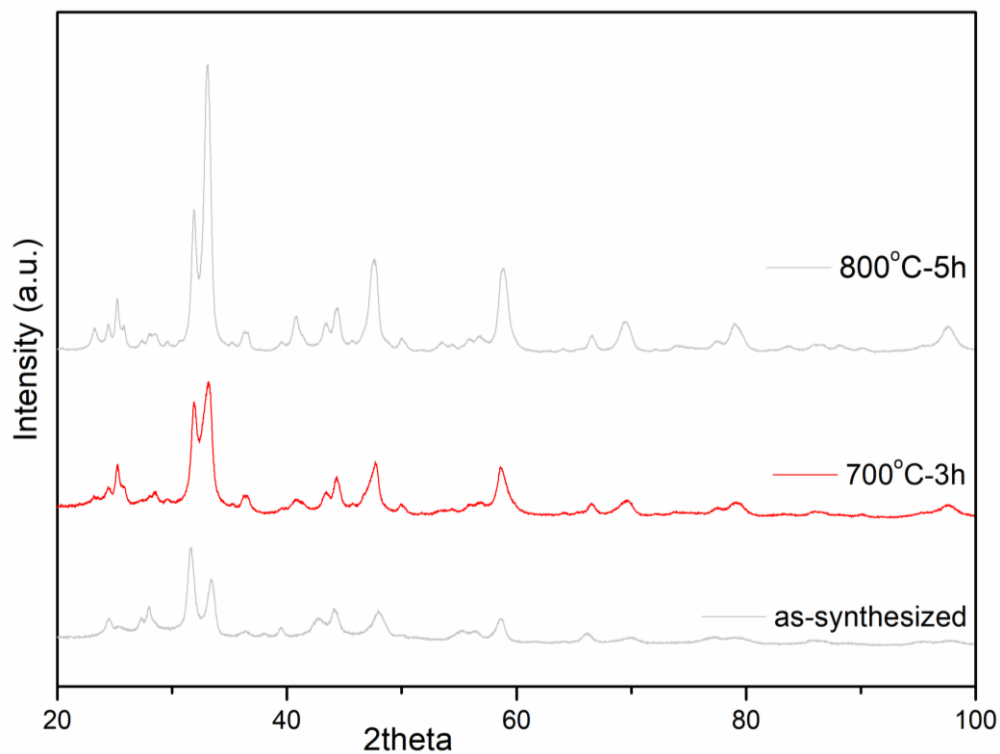


Figure 4.11. The relationship between the log(ASR) vs cycle number at constant temperatures

Measurements on the same sample was repeated three times, i.e. the same sample was heated up to 700°C. EIS measurements taken at 50°C interval. The sample was cooled to room temperature and the same measurement was repeated at the same interval while the sample was heated to 700°C. ASR values determined are plotted in Figure 4.11 at three selected temperatures. It is seen that the ASR values at constant temperature are quite close to each other. This implies that exposure to temperatures as high as 700°C does not lead to pronounced change in the structure.



*Figure 4.12.* X-ray diffractogram of powder synthesized by induction thermal plasma after 700°C 1hour annealing. XRD pattern of as-synthesized powder as well as that of powder annealed 800 °C for 5 hours are also included for comparison.

This was checked by annealing a new sample at 700°C for extended period of time, i.e. for 3 hours. XRD pattern of this annealed sample is shown in Figure 4.12. This pattern in as-synthesized sample and that recorded after annealing 800°C for 5 hours are also included in the Figure 4.12. It is seen that the pattern recorded at 700°C for 3 hours annealed are similar with as-synthesized powder. This shows that the structure is stable up to temperature of 700°C.



## CHAPTER 5

### CONCLUSION

The current study follows the previous work in which a superior performance was obtained in the composite cathode LSC-113/LSC-214 where the cathode was amorphous/nanocrystalline as a result of co-sputtering of the respective oxides. In the present work, similar compositions of cathodes were produced via thermal plasma and electrochemically characterized by impedance spectroscopy. As a result of the present work, the following conclusions can be drawn.

Nanopowders of LSC-113/LSC-214 can be synthesized via thermal plasma by feeding  $\text{La}(\text{NO}_3)_3 \cdot 6\text{H}_2\text{O}$ ,  $\text{Sr}(\text{NO}_3)_2$ ,  $\text{Co}(\text{NO}_3)_2 \cdot 6\text{H}_2\text{O}$  precursor solution. Nanopowders were 58 nm in size with a composition of LSC-113: LSC-214= 0.3:0.7 as verified with a Rietveld refined XRD pattern.

The potential of the powder as cathode material was tested on a symmetric cell where the powder was applied either side of the electrolyte (GDC) and tested with impedance spectroscopy. Measurement conducted over a wide range between 350- 700°C. This has shown that the area specific resistance value of  $\text{ASR}=0.15 \Omega \cdot \text{cm}^2$  can be obtained in the current cathodes at temperatures as low as 665°C. Moreover, ASR values measured in three cycles consecutively, were very similar to one another indicating that the cathode had a high thermal stability.

Area specific resistance values and the temperature where  $\text{ASR} = 0.15 \Omega \cdot \text{cm}^2$ , was obtained were comparable with those obtained with co-sputtered cathodes of similar composition. In sputter deposited cathode, which had a composition LSC113:LSC214=0.30:70, had ASR value of  $0.15 \Omega \cdot \text{cm}^2$  at 700°C. This temperature is quite close to the temperature obtained with the current work which was 665°C.

It is proposed that composite powder with LSC-113: LSC-214=0.50:0.50 composition is likely to have an improved area specific resistance, which make it possible to use the cathode at temperatures less than 600°C.

## REFERENCES

- [1] R. Doshi, "Development of Solid-Oxide Fuel Cells That Operate at 500°C," *J. Electrochem. Soc.*, vol. 146, no. 4, p. 1273, 1999.
- [2] G. Accardo, C. Ferone, R. Cioffi, D. Frattini, L. Spiridigliozzi, and G. Dell'Agli, "Electrical and microstructural characterization of ceramic gadolinium-doped ceria electrolytes for ITSOFCs by sol-gel route," *J. Appl. Biomater. Funct. Mater.*, vol. 14, no. 1, pp. e35–e41, 2016.
- [3] E. J. Crumlin *et al.*, "Surface strontium enrichment on highly active perovskites for oxygen electrocatalysis in solid oxide fuel cells," *Energy Environ. Sci.*, vol. 5, no. 3, p. 6081, 2012.
- [4] M. Sase *et al.*, "Enhancement of Oxygen Surface Exchange at the Hetero-interface of  $(\text{La,Sr})\text{CoO}_3/(\text{La,Sr})\text{CoO}_4$  with PLD-Layered Films," *J. Electrochem. Soc.*, vol. 155, no. 8, p. B793, 2008.
- [5] W. Ma *et al.*, "Vertically aligned nanocomposite  $\text{La}_{0.8}\text{Sr}_{0.2}\text{CoO}_3/(\text{La}_{0.5}\text{Sr}_{0.5})_2\text{CoO}_4$  cathodes – electronic structure, surface chemistry and oxygen reduction kinetics," *J. Mater. Chem. A*, vol. 3, no. 1, pp. 207–219, 2015.
- [6] D. Sari, F. Piskin, Z. C. Torunoglu, B. Yasar, Y. E. Kalay, and T. Ozturk, "Combinatorial development of nanocrystalline/amorphous  $(\text{La,Sr})\text{CoO}_3-(\text{La,Sr})_2\text{CoO}_4$  composite cathodes for IT-SOFCs," *Solid State Ionics*, vol. 326, no. October, pp. 124–130, 2018.
- [7] R. S. Lima and B. R. Marple, "Thermal spray coatings engineered from nanostructured ceramic agglomerated powders for structural, thermal barrier and biomedical applications: A review," *J. Therm. Spray Technol.*, vol. 16, no. 1, pp. 40–63, 2007.
- [8] D. Bouchard, L. Sun, F. Gitzhofer, and G. M. Brisard, "Synthesis and Characterization of  $\text{La}_{0.8}\text{Sr}_{0.2}\text{MO}_{3-\delta}$  (M = Mn, Fe, or Co) Cathode Materials by Induction Plasma Technology," *J. Therm. Spray Technol.*, vol. 15, no. 1, pp. 37–45, 2006.
- [9] M. Müller *et al.*, "Thermal induction plasma processes for the synthesis of SOFC materials," *Materwiss. Werksttech.*, vol. 33, no. 6, pp. 322–330, 2002.
- [10] Y. Shen, V. A. B. Almeida, and F. Gitzhofer, "Preparation of nanocomposite GDC/LSCF cathode material for IT-SOFC by induction plasma spraying," *J. Therm. Spray Technol.*, vol. 20, no. 1–2, pp. 145–153, 2011.
- [11] M. M. Kuklja, E. A. Kotomin, R. Merkle, Y. A. Mastrikov, and J. Maier, "Combined theoretical and experimental analysis of processes determining

- cathode performance in solid oxide fuel cells,” *Phys. Chem. Chem. Phys.*, vol. 15, no. 15, pp. 5443–5471, 2013.
- [12] A. Evans, A. Bieberle-Hütter, L. J. Bonderer, S. Stuckenholz, and L. J. Gauckler, “Micro-solid oxide fuel cells using free-standing 3 mol.% yttria-stabilised-tetragonal-zirconia-polycrystal electrolyte foils,” *J. Power Sources*, vol. 196, no. 23, pp. 10069–10073, 2011.
- [13] H. J. Choi, K. Bae, D. Y. Jang, J. W. Kim, and J. H. Shim, “Performance Degradation of Lanthanum Strontium Cobaltite after Surface Modification,” *J. Electrochem. Soc.*, vol. 162, no. 6, pp. F622–F626, 2015.
- [14] B. C. H. Steele and A. Heinzl, “Materials for fuel-cell technologies,” vol. 414, no. November, pp. 345–352, 2001.
- [15] C. Sun, R. Hui, and J. Roller, “Cathode materials for solid oxide fuel cells: A review,” *J. Solid State Electrochem.*, vol. 14, no. 7, pp. 1125–1144, 2010.
- [16] N. Mahato, A. Banerjee, A. Gupta, S. Omar, and K. Balani, “Progress in material selection for solid oxide fuel cell technology: A review,” *Prog. Mater. Sci.*, vol. 72, pp. 141–337, 2015.
- [17] S. P. S. Shaikh, A. Muchtar, and M. R. Somalu, “A review on the selection of anode materials for solid-oxide fuel cells,” *Renew. Sustain. Energy Rev.*, vol. 51, pp. 1–8, 2015.
- [18] M. R. Somalu, A. Muchtar, W. R. W. Daud, and N. P. Brandon, “Screen-printing inks for the fabrication of solid oxide fuel cell films: A review,” *Renew. Sustain. Energy Rev.*, vol. 75, no. December 2015, pp. 426–439, 2017.
- [19] W. Z. Zhu and S. C. Deevi, “A review on the status of anode materials for solid oxide fuel cells,” *Mater. Sci. Eng. A*, vol. 362, no. 1–2, pp. 228–239, 2003.
- [20] X. Ge *et al.*, “Screen-printed thin YSZ films used as electrolytes for solid oxide fuel cells,” *J. Power Sources*, vol. 159, no. 2, pp. 1048–1050, 2006.
- [21] Y. Lee, Y. M. Park, and G. M. Choi, “Micro-solid oxide fuel cell supported on a porous metallic Ni/stainless-steel bi-layer,” *J. Power Sources*, vol. 249, pp. 79–83, 2014.
- [22] H. Kim, C. Lu, W. L. Worrell, J. M. Vohs, and R. J. Gorte, “Cu-Ni Cermet Anodes for Direct Oxidation of Methane in Solid-Oxide Fuel Cells,” *J. Electrochem. Soc.*, vol. 149, no. 3, p. A247, 2002.
- [23] E. J. Crumlin *et al.*, “Oxygen reduction kinetics enhancement on a heterostructured oxide surface for solid oxide fuel cells,” *J. Phys. Chem. Lett.*, 2010.
- [24] J. B. Goodenough and Y. H. Huang, “Alternative anode materials for solid oxide fuel cells,” *J. Power Sources*, vol. 173, no. 1, pp. 1–10, 2007.

- [25] J. H. Song, S. Il Park, J. H. Lee, and H. S. Kim, "Fabrication characteristics of an anode-supported thin-film electrolyte fabricated by the tape casting method for IT-SOFC," *J. Mater. Process. Technol.*, vol. 198, no. 1–3, pp. 414–418, 2008.
- [26] L. Zhang, R. Lan, C. T. G. Petit, and S. Tao, "Durability study of an intermediate temperature fuel cell based on an oxide-carbonate composite electrolyte," *Int. J. Hydrogen Energy*, vol. 35, no. 13, pp. 6934–6940, 2010.
- [27] R. J. Gorte, S. Park, J. M. Vohs, and C. Wang, "Anodes for direct oxidation of dry hydrocarbons in a solid-oxide fuel cell," *Adv. Mater.*, vol. 12, no. 19, pp. 1465–1469, 2000.
- [28] P. Scribe *et al.*, "Double Perovskites as Anode Materials for SOFCs," vol. 312, no. April, pp. 251–254, 2006.
- [29] B. C. H. Steele, "Survey of materials selection for ceramic fuel cells: II. Cathodes and anodes," *Solid State Ionics*, vol. 86–88, no. PART 2, pp. 1223–1234, 1996.
- [30] K. Nikooyeh, R. Clemmer, V. Alzate-Restrepo, and J. M. Hill, "Effect of hydrogen on carbon formation on Ni/YSZ composites exposed to methane," *Appl. Catal. A Gen.*, vol. 347, no. 1, pp. 106–111, 2008.
- [31] J. F. B. Rasmussen and A. Hagen, "The effect of H<sub>2</sub>S on the performance of Ni-YSZ anodes in solid oxide fuel cells," *J. Power Sources*, vol. 191, no. 2, pp. 534–541, 2009.
- [32] M. Biswas and K. C. Sadanala, "Electrolyte Materials for Solid Oxide Fuel Cell," *J. Powder Metall. Min.*, vol. 02, no. 04, pp. 10–15, 2017.
- [33] B. C. H. Steele, "Material science and engineering: The enabling technology for the commercialisation of fuel cell systems," *J. Mater. Sci.*, vol. 36, no. 5, pp. 1053–1068, 2001.
- [34] J. A. Kilner and M. Burriel, "Materials for Intermediate-Temperature Solid-Oxide Fuel Cells," *Annu. Rev. Mater. Res.*, vol. 44, no. 1, pp. 365–393, 2014.
- [35] A. Endo, "Low Overvoltage Mechanism of High Ionic Conducting Cathode for Solid Oxide Fuel Cell," *J. Electrochem. Soc.*, vol. 145, no. 3, p. L35, 2006.
- [36] N. Q. Minh, *Science and Technology of Ceramic Fuel Cells*. Elsevier, 1995.
- [37] J. W. Fergus, "Materials challenges for solid-oxide fuel cells," *Jom*, vol. 59, no. 12, pp. 56–62, 2007.
- [38] G. Y. Cho *et al.*, "High-performance thin film solid oxide fuel cells with scandia-stabilized zirconia (ScSZ) thin film electrolyte," *Int. J. Hydrogen Energy*, vol. 40, no. 45, pp. 15704–15708, 2015.

- [39] S. P. S. Badwal, "Stability of solid oxide fuel cell components," *Solid State Ionics*, vol. 143, no. 1, pp. 39–46, 2001.
- [40] L. Malavasi, C. A. J. Fisher, and M. S. Islam, "Oxide-ion and proton conducting electrolyte materials for clean energy applications: Structural and mechanistic features," *Chem. Soc. Rev.*, vol. 39, no. 11, pp. 4370–4387, 2010.
- [41] W. Gong, S. Gopalan, and U. B. Pal, "Performance of intermediate temperature (600–800 °C) solid oxide fuel cell based on Sr and Mg doped lanthanum-gallate electrolyte," *J. Power Sources*, vol. 160, no. 1, pp. 305–315, 2006.
- [42] G. Y. Meng, Q. X. Fu, S. W. Zha, C. R. Xia, X. Q. Liu, and D. K. Peng, "Novel intermediate temperature ceramic fuel cells with doped ceria-based composite electrolytes," *Solid State Ionics*, vol. 148, no. 3–4, pp. 533–537, 2002.
- [43] A. J. Jacobson, "Materials for solid oxide fuel cells," *Recent Trends Fuel Cell Sci. Technol.*, pp. 286–331, 2007.
- [44] A. Chroneos, B. Yildiz, A. Tarancón, D. Parfitt, and J. A. Kilner, "Oxygen diffusion in solid oxide fuel cell cathode and electrolyte materials: Mechanistic insights from atomistic simulations," *Energy Environ. Sci.*, vol. 4, no. 8, pp. 2774–2789, 2011.
- [45] J. Fleig and J. Maier, "The polarization of mixed conducting SOFC cathodes: Effects of surface reaction coefficient, ionic conductivity and geometry," *J. Eur. Ceram. Soc.*, vol. 24, no. 6, pp. 1343–1347, 2004.
- [46] B. A. Boukamp, N. Hildenbrand, H. J. M. Bouwmeester, and D. H. A. Blank, "Impedance of thin film cathodes: Thickness and current collector dependence," *Solid State Ionics*, vol. 283, pp. 81–90, 2015.
- [47] C. Sun, R. Hui, and J. Roller, "Cathode materials for solid oxide fuel cells: A review," *J. Solid State Electrochem.*, vol. 14, no. 7, pp. 1125–1144, 2010.
- [48] A. Tarancón, M. Burriel, J. Santiso, S. J. Skinner, and J. A. Kilner, "Advances in layered oxide cathodes for intermediate temperature solid oxide fuel cells," *J. Mater. Chem.*, vol. 20, no. 19, p. 3799, 2010.
- [49] B. C. H. Steele, "Appraisal of  $\text{Ce}_{1-y}\text{Gd}_y\text{O}_{2-y/2}$  electrolytes for IT-SOFC operation at 500 °C," *Solid State Ionics*, vol. 129, no. 1, pp. 95–110, 2000.
- [50] H. Yokokawa, H. Tu, B. Iwanschitz, and A. Mai, "Fundamental mechanisms limiting solid oxide fuel cell durability," *J. Power Sources*, vol. 182, no. 2, pp. 400–412, 2008.
- [51] F. Tietz, Q. Fu, V. A. C. Haanappel, A. Mai, N. H. Menzler, and S. Uhlenbruck, "Materials development for advanced planar solid oxide fuel cells," *Int. J. Appl. Ceram. Technol.*, vol. 4, no. 5, pp. 436–445, 2007.

- [52] A. Mai *et al.*, “Time-dependent performance of mixed-conducting SOFC cathodes,” *Solid State Ionics*, vol. 177, no. 19-25 SPEC. ISS., pp. 1965–1968, 2006.
- [53] M. Sase *et al.*, “Enhancement of oxygen exchange at the hetero interface of (La,Sr)CoO<sub>3</sub>/(La,Sr)<sub>2</sub>CoO<sub>4</sub> in composite ceramics,” *Solid State Ionics*, vol. 178, no. 35–36, pp. 1843–1852, 2008.
- [54] B. Wei *et al.*, “Crystal structure, thermal expansion and electrical conductivity of perovskite oxides Ba<sub>x</sub>Sr<sub>1-x</sub>Co<sub>0.8</sub>Fe<sub>0.2</sub>O<sub>3-δ</sub> (0.3 ≤ x ≤ 0.7),” *J. Eur. Ceram. Soc.*, vol. 26, no. 13, pp. 2827–2832, 2006.
- [55] M. Zinkevich and F. Aldinger, “Thermodynamic analysis of the ternary La-Ni-O system,” *J. Alloys Compd.*, vol. 375, no. 1–2, pp. 147–161, 2004.
- [56] R. Chiba, F. Yoshimura, and Y. Sakurai, “Properties of La<sub>1-y</sub>Sr<sub>y</sub>Ni<sub>1-x</sub>Fe<sub>x</sub>O<sub>3</sub> as a cathode material for a low-temperature operating SOFC,” *Solid State Ionics*, vol. 152–153, pp. 575–582, 2002.
- [57] E. V. Tsipis, E. A. Kiselev, V. A. Kolotygin, J. C. Waerenborgh, V. A. Cherepanov, and V. V. Kharton, “Mixed conductivity, Mössbauer spectra and thermal expansion of (La,Sr)(Fe,Ni)O<sub>3-δ</sub> perovskites,” *Solid State Ionics*, vol. 179, no. 38, pp. 2170–2180, 2008.
- [58] R. Chiba, F. Yoshimura, and Y. Sakurai, “Investigation of LaNi<sub>1-x</sub>Fe<sub>x</sub>O<sub>3</sub> as a cathode material for solid oxide fuel cells,” *Solid State Ionics*, vol. 124, no. 3, pp. 281–288, 1999.
- [59] H. Orui, K. Watanabe, R. Chiba, and M. Arakawa, “Application of LaNi(Fe)O<sub>3</sub> as SOFC Cathode,” *J. Electrochem. Soc.*, vol. 151, no. 9, p. A1412, 2004.
- [60] T. Komatsu, H. Arai, R. Chiba, K. Nozawa, M. Arakawa, and K. Sato, “Cr Poisoning Suppression in Solid Oxide Fuel Cells Using LaNi(Fe)O<sub>3</sub> Electrodes,” *Electrochem. Solid-State Lett.*, vol. 9, no. 1, p. A9, 2006.
- [61] T. Komatsu, H. Arai, R. Chiba, K. Nozawa, M. Arakawa, and K. Sato, “Long-Term Chemical Stability of LaNi(Fe)O<sub>3</sub> as a Cathode Material in Solid Oxide Fuel Cells,” *J. Electrochem. Soc.*, vol. 154, no. 4, p. B379, 2007.
- [62] O. Yamamoto, Y. Takeda, R. Kanno, and M. Node, “Perovskite-Type Oxides as Oxygen Electrodes For High Temperature Oxide Fuel Cells,” vol. 0182, no. 86, pp. 1–18, 1986.
- [63] A. Weber and E. Ivers-Tiffée, “Materials and concepts for solid oxide fuel cells (SOFCs) in stationary and mobile applications,” *J. Power Sources*, vol. 127, no. 1–2, pp. 273–283, 2004.
- [64] V. V. Sikolenko, E. V. Pomjakushina, and S. Y. Istomin, “Neutron diffraction

- studies of  $\text{La}_{1-x}\text{Sr}_x\text{CoO}_3$  magnetic structure at  $x = 0.15$  and  $0.3$ ,” *J. Magn. Mater.*, vol. 258–259, pp. 300–301, 2003.
- [65] A. Das, S. K. Paranjpe, P. A. Joy, and S. K. Date, “Neutron depolarization and diffraction studies in cluster glass  $\text{La}_{0.5}\text{Sr}_{0.5}\text{CoO}_3$ ,” vol. 326, pp. 101–104, 2001.
- [66] M. Sánchez-Andújar and M. A. Senaris-Rodríguez, “Synthesis, structure and microstructure of the layered compounds  $\text{Ln}_{1-x}\text{Sr}_{1+x}\text{CoO}_4$  (Ln: La, Nd and Gd),” *Solid State Sci.*, vol. 6, no. 1, pp. 21–27, 2004.
- [67] M. James, A. Tedesco, D. Cassidy, M. Colella, and P. J. Smythe, “The phase diagram and crystal chemistry of strontium-doped rare earth cobaltates:  $\text{Ln}_{2-x}\text{Sr}_x\text{CoO}_{4+\delta}$  (Ln = La-Dy),” *J. Alloys Compd.*, vol. 419, no. 1–2, pp. 201–207, 2006.
- [68] H. M. Rietveld, “A profile refinement method for nuclear and magnetic structures,” *J. Appl. Crystallogr.*, vol. 2, no. 2, pp. 65–71, 1969.
- [69] J. Chen *et al.*, “Nano-structured (La, Sr)(Co, Fe) $\text{O}_3$  + YSZ composite cathodes for intermediate temperature solid oxide fuel cells,” *J. Power Sources*, vol. 183, no. 2, pp. 586–589, 2008.
- [70] H. J. Ko, J. H. Myung, J. H. Lee, S. H. Hyun, and J. S. Chung, “Synthesis and evaluation of  $(\text{La}_{0.6}\text{Sr}_{0.4})(\text{Co}_{0.2}\text{Fe}_{0.8})\text{O}_3$  (LSCF)- $\text{Y}_{0.08}\text{Zr}_{0.92}\text{O}_{1.96}$  (YSZ)- $\text{Gd}_{0.1}\text{Ce}_{0.9}\text{O}_{2-\delta}$  (GDC) dual composite SOFC cathodes for high performance and durability,” *Int. J. Hydrogen Energy*, vol. 37, no. 22, pp. 17209–17216, 2012.
- [71] Y. Leng, S. H. Chan, and Q. Liu, “Development of LSCF-GDC composite cathodes for low-temperature solid oxide fuel cells with thin film GDC electrolyte,” *Int. J. Hydrogen Energy*, vol. 33, no. 14, pp. 3808–3817, 2008.
- [72] E. P. Murray and S. A. Barnett, “ $(\text{La,Sr})\text{MnO}_3$ - $(\text{Ce,Gd})\text{O}_{2-x}$  composite cathodes for SOFCs,” pp. 265–273, 2001.
- [73] Z. Feng *et al.*, “In situ studies of the temperature-dependent surface structure and chemistry of single-crystalline (001)-oriented  $\text{La}_{0.8}\text{Sr}_{0.2}\text{CoO}_{3-\delta}$  perovskite thin films,” *J. Phys. Chem. Lett.*, vol. 4, no. 9, pp. 1512–1518, 2013.
- [74] K. Yashiro *et al.*, “Composite Cathode of Perovskite-Related Oxides,  $(\text{La,Sr})\text{CoO}_{3-\delta}/(\text{La,Sr})_2\text{CoO}_{4-\delta}$ , for Solid Oxide Fuel Cells,” *Electrochem. Solid-State Lett.*, vol. 12, no. 9, p. B135, 2009.
- [75] E. J. Crumlin *et al.*, “Oxygen reduction kinetics enhancement on a heterostructured oxide surface for solid oxide fuel cells,” *J. Phys. Chem. Lett.*, vol. 1, no. 21, pp. 3149–3155, 2010.
- [76] E. Mutoro, E. J. Crumlin, M. D. Biegalski, H. M. Christen, and Y. Shao-Horn,

- “Enhanced oxygen reduction activity on surface-decorated perovskite thin films for solid oxide fuel cells,” *Energy Environ. Sci.*, vol. 4, no. 9, pp. 3689–3696, 2011.
- [77] D. Lee, Y. L. Lee, W. T. Hong, M. D. Biegalski, D. Morgan, and Y. Shao-Horn, “Oxygen surface exchange kinetics and stability of  $(\text{La,Sr})_2\text{CoO}_{4\pm\delta}/\text{La}_{1-x}\text{Sr}_x\text{MO}_{3-\delta}$  ( $M = \text{Co}$  and  $\text{Fe}$ ) hetero-interfaces at intermediate temperatures,” *J. Mater. Chem. A*, vol. 3, no. 5, pp. 2144–2157, 2015.
- [78] and H.-R. W. L. Lutterotti, S. Matthies, “MAUD: a friendly Java program for material analysis using diffraction,” *IUCr Newsl. CPD*, vol. 21, pp. 14–15, 1999.
- [79] M. R. Somalu, V. Yufit, I. P. Shapiro, P. Xiao, and N. P. Brandon, “The impact of ink rheology on the properties of screen-printed solid oxide fuel cell anodes,” *Int. J. Hydrogen Energy*, vol. 38, no. 16, pp. 6789–6801, 2013.
- [80] P. Ried *et al.*, “Processing of YSZ screen printing pastes and the characterization of the electrolyte layers for anode supported SOFC,” *J. Eur. Ceram. Soc.*, vol. 28, no. 9, pp. 1801–1808, 2008.
- [81] R. Hansch, M. R. R. Chowdhury, and N. H. Menzler, “Screen printing of sol-gel-derived electrolytes for solid oxide fuel cell (SOFC) application,” *Ceram. Int.*, vol. 35, no. 2, pp. 803–811, 2009.
- [82] J. Januschewsky, M. Ahrens, A. Opitz, F. Kubel, and J. Fleig, “Optimized  $\text{La}_{0.6}\text{Sr}_{0.4}\text{CoO}_3$  thin-film electrodes with extremely fast oxygen-reduction kinetics,” *Adv. Funct. Mater.*, vol. 19, no. 19, pp. 3151–3156, 2009.
- [83] S. Maitra, N. Chakrabarty, and J. Pramanik, “Decomposition kinetics of alkaline earth carbonates by integral approximation method,” *Ceramica*, vol. 54, no. 331, pp. 268–272, 2008.
- [84] A. Cavallaro *et al.*, “Electronic nature of the enhanced conductivity in YSZ-STO multilayers deposited by PLD,” *Solid State Ionics*, vol. 181, no. 13–14, pp. 592–601, 2010.
- [85] K. Yamahara, C. P. Jacobson, S. J. Visco, X. F. Zhang, and L. C. De Jonghe, “Thin film SOFCs with cobalt-infiltrated cathodes,” *Solid State Ionics*, 2005.
- [86] A. Aguadero *et al.*, “Materials development for intermediate-temperature solid oxide electrochemical devices,” *J. Mater. Sci.*, vol. 47, no. 9, pp. 3925–3948, 2012.

